Molecular Packing in Cylindrical Micelles

S. May[a] **and A. Ben-Shaul**[b]

[a] Department of Physics, North Dakota State University, Fargo ND, 58105 USA

[b]Department of Physical Chemistry and the Fritz Haber Research Center,
The Hebrew University, Jerusalem 91904, Israel

I. Introduction

The elongated shape of linear, worm-like, micelles is among the most common aggregation geometries of amphiphilic molecules in aqueous solutions. The cylindrical body of these uni-dimensional micelles can be regarded as an intermediate packing geometry, of a higher *growth dimensionality* than that of a spherical micelle and lower than that of a planar bilayer. In all these three canonical structures, the hydrophobic tails of the constituent amphiphiles form a compact, liquid-like, hydrocarbon core, with their polar headgroups residing on its surface, thus largely shielding the hydrocarbon tails from direct contact with water. The planar bilayer is a two dimensional (2D) object; it can grow laterally along $d = 2$ directions, but its third dimension is always microscopic. Namely, its thickness, or, more precisely, the distance ($2b$) between its two hydrocarbon-water interfaces cannot exceed $2b_{max}$, where b_{max} is the length of the fully extended hydrocarbon tail. Similarly, the growth dimensionality of a worm-like micelle is $d = 1$. It can elongate along the cylindrical axis, but its diameter ($2b$) – and hence the two perpendicular dimensions – cannot exceed $2b_{max}$. The growth dimensionality of a spherical micelle (keeping its spherical symmetry) is, of course, $d = 0$, since to maintain a compact hydrophobic core all its three dimensions must be smaller than ($2b_{max}$. Note that this last statement is only relevant to systems where a spherical micelle is the intrinsically preferred (or, referred 'spontaneous') packing environment of the amphiphiles. As briefly discussed later in this chapter, many other amphiphiles, in fact most of those that prefer packing into long cylindrical micelles, first assemble – for entropic reasons – into small spherical micelles. However, above the *critical micelle concentration* (CMC), driven by the lower packing energy in the cylindrical geometry, the added amphiphiles incorporate into the middle of the aggregate, forming a gradually elongating cylindrical mid-section, capped by two approximately hem-spherical micellar caps. In these systems the spherical micelle is just the low concentration limit of a linear aggregate.

The reversible self-assembly of amphiphiles in aqueous environments is a fundamental processes, omnipresent in living organisms and underlying numerous technological applications.[1] Thermodynamically, micellar solutions belong to the wider class of systems known as complex fluids.[2,3] One of the special characteristics of these solutions is that the solute particles, unlike in ordinary molecular solutions, can modify their size, shape and even their aggregation geometry. Such changes occur generally in response to varying ambient conditions, like the total concentration, temperature or ionic strength. For instance, upon increasing the amphiphile concentration in a solution of cylindrical ('rodlike') micelles, the average micelle size increases monotonically, resulting in substantial inter-micelle interactions. Eventually, these interactions become strong enough to drive a transition from an isotropic to a nematic phase of rodlike aggregates. However, unlike in ordinary liquid crystalline solutions, the micelle size in the nematic phase is much larger than in the coexisting isotropic phase, demonstrating a subtle coupling between the inter-molecular (or, intra-aggregate) and inter-micelle interactions.[4] This coupling arises because the (non-covalent) forces holding together the amphiphiles in a micelle are relatively weak, typically on the order of k_BT per molecule, where

k_B is Boltzmann's constant and T is the absolute temperature. At high total amphiphile concentrations inter-aggregate interactions, often dominated by packing (excluded volume) interactions of entropic origin, may be of comparable magnitude, and thus induce structural and morphological changes of the aggregates. There are many examples for the coupling between inter-molecular and inter-aggregate interactions besides the isotropic-nematic transition of rodlike micelles mentioned above. These include, for instance, the formation of branched micelles and inter-connected phases resembling polymer gels, or the transition between lamellar and bicontinuous ('sponge') phases in surfactant solutions.[3,4]

Above the CMC but still in the dilute solution regime, adding amphiphiles to a micellar solution of (intrinsically preferred) spherical micelles, will simply result in the formation of new micelles, all of the same size. On the other hand, amphiphiles whose intrinsically preferred aggregation geometry is the planar bilayer, will spontaneously assemble into macroscopic bilayer sheets. This process, which typically occurs already at extremely small amphiphile concentrations is, in fact, a first order transition from a very dilute phase of isolated amphiphiles into a condensed 2D bilayer phase. As compared to these two cases, the phase behavior associated with amphiphiles whose spontaneous aggregation geometry is cylindrical is considerably more interesting, even in dilute solution. Like other 1D systems, linear molecular aggregation is a continuous, gradual, process, as opposed to a first order phase transition. That is, the average micellar size increases with the total concentration, yet it is always finite. Although this topic has been intensively discussed in the literature, including in other chapters in this volume, we shall briefly review its basic thermodynamic aspects in the next section, mainly in order to emphasize the intimate relationship between structural-molecular characteristics of amphiphile organization to the thermodynamics of micelle formation and growth.

Most chapters in this volume are concerned with the structural, rheological and thermodynamic characteristics of giant, "worm-like", micelles. Once the size of these micelles exceeds the persistence length of a cylindrical micelle, their conformational behavior is similar to that of flexible polymers. We note, however, that owing to the reversible nature of amphiphile assembly worm-like micelles are "living polymers". As noted above, they can form and break in response to inter-micelle interactions, as well as external fields, e.g., flow fields. The self-assembled nature of worm-like micelles thus affects many physical properties, and contributes to a remarkable rheological behavior of their solutions.[5] The structure and stability of these micelles, as well as their growth characteristics, flexibility, and ability to form inter-micellar junctions (as observed in certain systems) depend on the intermolecular interactions governing their packing into micellar aggregates. These, molecular, aspects of amphiphile assembly are in the focus of the present chapter.

Worm-like micelles are formed by numerous ionic and non-ionic, single tailed surfactants, but also by certain double-tailed amphiphiles,[6] as well as diblock copolymers.[7] Nonionic micelles are not subject to the many complications that arise due to the long range nature of electrostatic interactions. Yet, in the case of ionic surfactants one can regulate the preferred aggregation geometry by varying the nature of the counterions or the salt content in solution. Frequently, the growth of ionic micelles can be enhanced by adding a large amount of salt; but certain worm-like micelles also exist under salt free conditions.[8,9] Because charged worm-like micelles bear similarities to polyelectrolytes,[10] concepts developed for charged polymers, such as the electrostatic contribution to the persistence length,[11,12] can often be applied to worm-like micelles. As noted above, however, differences arise from the self-assembled nature of the micelles, and hence their ability to adjust their length distribution, to form transient junctions or even to cross each other (ghost crossing). In the last section of this chapter we shall briefly discuss the effects of electrostatic interactions on the properties of linear micelles.

The tail region of amphiphiles consists typically of one or more short hydrocarbon chains. In a spherical micelle the hydrocarbon tail occupies, on average, a cone like section of the hydrophobic core, whose base is at the hydrocarbon-water interface and whose tip is in the center of the micelle. Similarly, the average

shape of the tail volume in a cylindrical micelle is wedge-like and in a planar bilayer it is cylindrical. Other average shapes characterize more complex structures, such as the saddle geometry encountered in certain inverted phases and intermicellar junctions. In bilayers above the chain-melting transition temperature, and in all micellar aggregates, the hydrocarbon tails are thermally excited, fluctuating between numerous accessible chain conformations. This conformational flexibility is responsible for the ability of amphiphiles to form a surprisingly large variety of aggregate geometries, including micelles, membranes and bicontinuous structures.[1,3,4] Owing to this conformational freedom the tails enable the formation of uniform, liquid-like, hydrocarbon cores for all these aggregation geometries. In the simplest phenomenological theory of amphiphile self-assembly, known as the opposing forces model (OFM),[13,14] this is known as *the hydrocarbon droplet assumption*. In fact, in this model it is further assumed that, owing to the liquid-like nature of the hydrophobic core, the packing free energy of the tails is independent of the aggregation geometry; namely, it is the same, for instance, in a cylindrical micelle and a planar bilayer. Following this assumption the preferred aggregation geometry in dilute solution, or, in other words, the spontaneous packing curvature of amphiphiles in a micellar aggregate, is dictated by the balance of two forces, both operative at the micelle's interfacial region. These, opposing forces, are i) the repulsion between amphiphile headgroups which tend to maximize the interfacial area per molecule, and ii) the hydrocarbon-water surface energy, which acts in the opposite direction.

The OFM picture provides a convincing qualitative explanation to various self-assembly phenomena. For example, the preference of strongly charged surfactants to form curved micelles, or the tendency of double-tailed phospholipids to assemble into lipid membranes.[13,14] On the other hand, in order to account for certain, more subtle though no less important properties of micellar aggregates, one must take into account the different packing constraints imposed on the *hydrocarbon tails* in different packing geometries. This central role of chain conformational statistics in determining the curvature elastic properties of lipid membranes is one familiar example.[15] In the following sections we shall show that conformational chain packing statistics is also crucial for explaining the *bending elasticity* of worm-like micelles, the energetics of *inter-micellar junctions*, and the *second CMC* observed in various micellar solutions. Our approach for treating the conformational properties of amphiphile chains in the hydrophobic cores of different micellar geometries is based on a mean field, molecular-level, theory which has been widely applied to various issues pertaining to amphiphile self-assembly, including the topics highlighted above.

II. Micellar aggregation thermodynamics

In this section we briefly outline the thermodynamics of amphiphile self-assembly in dilute solution. The system of interest is an aqueous solution of volume V, containing M amphiphiles, in both monomeric and aggregated form. In the the dilute solution regime $M \ll M_w$ is much smaller than the number, M_w, of solvent (water) molecules. We shall use M_1 to denote the number of monomeric amphiphiles in solution, and M_N ($N \geq 2$) for the number of aggregates of aggregation number N. Thus, M_2 is the number of dimers, M_3 the number of trimers, etc. On the other hand, NM_N is the total number of molecules incorporated into aggregates comprising $N \geq 2$ amphiphiles. (In micellar solutions, as discussed in the next section, there is typically a minimal aggregation number, $\bar{N}$, so that aggregates of intermediate sizes, $2 \leq N \leq \bar{N}$ are highly unlikely to appear in solution.) It is common to express the aggregate size distribution on the *mole fraction* scale, $X_N = NM_N/\mathcal{M}$, where in the dilute solution limit $\mathcal{M} = M_w + M \approx V/\nu_w$, where ν_w is the volume per molecule in pure water. The sum $\sum_{N=1}^{\infty} X_N = X$, is, of course, the overall mole fraction of amphiphiles in solution, $X = M/\mathcal{M}$.

The Helmholtz free energy, $F = F[\{X_N\}]$, corresponding to any given distribution, $\{X_N\}$, of aggregate

sizes is given by[1,3,15]

$$F = \mathcal{M} \sum_{N=1}^{\infty} \left[X_N \tilde{\mu}_N^0 + k_B T \frac{X_N}{N} \left(\ln \frac{X_N}{N} - 1 \right) \right] \tag{1}$$

where $\tilde{\mu}_N^0$ is the standard chemical potential per amphiphile in an aggregate of size N. The second term in the sum, or more precisely $-k_B(M_N/\mathcal{M})[\ln(M_N/\mathcal{M}) - 1]$, (note $M_N/\mathcal{M} = X_N/N$), is the translational entropy of micelles of size N in solution. The sum of these terms is the contribution of (monomeric amphiphiles and micelles) to the mixing entropy of the solution. Note that Eq. 1 does not include the contribution of the solvent to the free energy (namely, $M_w[\tilde{\mu}_w^0 + k_B T X_w \ln X_w]$), because in the dilute solution limit this is a constant, independent of $\{X_N\}$. It may also be noted that $\mu_N^0 - N\tilde{\mu}_1^0 = N[\tilde{\mu}_N^0 - \tilde{\mu}_1^0]$, is the standard free energy of formation of an N-micelle from N monomers. Physically, this is the packing free energy of the N-amphiphiles into a micelle, measured with respect to the state of a fully dissociated aggregate.

Eq. 1 is valid for any multicomponent solution of (fixed) composition $\{X_N\}$. In a solution of self-assembling molecules, all association-dissociation "reactions" are possible, e.g., $\mathcal{A}_N \rightleftharpoons \mathcal{A}_m + \mathcal{A}_{N-m}$ etc., where $\mathcal{A}_m$ denotes a micelle of m amphiphiles. The equilibrium (or, equivalently the most probable) distribution of average micellar sizes, $\{X_N^{eq}\}$, is the one which minimizes $F = F[\{X_N\}]$, subject to the condition of conserving the overall number of amphiphiles, M,

$$\sum_{N=1}^{\infty} X_N = X = constant \tag{2}$$

The resulting, equilibrium, distribution is

$$X_N = N \exp\left[-N(\tilde{\mu}_N^0 - \mu)/k_B T\right] \tag{3}$$

where μ is the Lagrangian multiplier conjugate to the conservation constraint Eq. 2; and where for notational brevity we have omitted the superscript '*eq*'. As in any macroscopic system, fluctuations of the X_N around their equilibrium values are negligible.

Substituting the equilibrium distribution, Eq. 3, back into Eq. 1 we obtain

$$\frac{F}{\mathcal{M}} = \mu X - k_B T \sum_{N=1}^{\infty} \frac{X_N}{N} \tag{4}$$

The osmotic pressure of the micellar solution is $\Pi = -\partial F/\partial V = k_B T \sum_{N=1}^{\infty} M_N/V$, where the second equality is valid in the dilute solution limit. Thus, Eq. 4 is the familiar relation, $F = G - \Pi V$, between the Helmholtz free energy, F, and Gibbs free energy, $G = \mu M$, of the solution, (again, apart from the constant part of the solvent).

The chemical potential per amphiphile in an N-mer is $\tilde{\mu}_N = \partial(F/\mathcal{M})/\partial X_N$, which, using Eq. 1 yields $\tilde{\mu}_N = \tilde{\mu}_N^0 + (k_B T/N)\ln(X_N/N)$. At equilibrium, the chemical potential of all amphiphiles in solution should be independent of their state of aggregation, just like in phase equilibrium. Indeed, from Eq. 3 it follows that

$$\tilde{\mu}_N = \tilde{\mu}_N^0 + (k_B T/N)\ln(X_N/N) = \mu, \qquad (\text{all } N) \tag{5}$$

is a constant, $\tilde{\mu}_N = \mu$, for all N. As expected, this result confirms that the Lagrangian multiplier μ conjugate to the conservation condition of the number of amphiphiles (Eq. 2) is, indeed, the chemical potential of *all* amphiphiles present in solution. Replacing μ by $\tilde{\mu}_1 = \tilde{\mu}_1^0 + k_B T \ln X_1$ in Eq. 3 we find

$$\frac{X_N/N}{X_1^N} = \exp\left[-\frac{N}{k_B T} \left(\tilde{\mu}_1^0 - \tilde{\mu}_N^0 \right) \right] \tag{6}$$

This expression is the familiar mass action law applied to the chemical reaction $N\mathcal{A}_1 \rightleftharpoons \mathcal{A}_N$.[13] Of course, this does not imply that micelle formation requires the simultaneous association of N monomers. Analogous expressions apply to any other set of such reactions, e.g., $\mathcal{A}_{N-1} + \mathcal{A}_1 \rightleftharpoons \mathcal{A}_N$.

In the two following sections we briefly discuss how the dependence of $\tilde{\mu}_N^0$ on N dictates the cooperative formation of micelles from monomers at the *critical micelle concentration*, and their subsequent growth into elongated cylindrical aggregates.

A. The CMC

In the limit of very low concentrations, the amphiphiles in solution are monomeric. Above a certain threshold critical concentration, the CMC, globular micelles composed typically of 30-100 molecules appear in solution, while the concentration of monomers remains essentially constant. (In the case of bilayer forming molecules, e.g., phospholipids, the transition generally occurs at vanishingly small concentrations, and directly to macroscopic aggregates.) As noted already in the introduction, if spherical micelles present the optimal packing geometry, then increasing the concentration above the CMC will result in the formation of additional micelles of this shape. On the other hand, if cylindrical packing is preferred, the globular micelles will gradually elongate into longer ones as the overall concentration increases. The cooperative nature of micelle formation at the CMC is a direct reflection of the existence of some minimal aggregation number $\bar{N}$, such that aggregates containing less than (about) $\bar{N}$ molecules are unstable, and thus either dissociate into monomers or associate to form $N \geq \bar{N}$-aggregates. To a first approximation $\bar{N}$ is dictated by the size of a spherical micelle enabling amphiphile packing at their optimal area per headgroup. More formally, the existence of a minimal aggregation number is due to the fact that $\tilde{\mu}_N^0 \gg \tilde{\mu}_{\bar{N}}^0$ for all $N < \bar{N}$.

To demonstrate the cooperative behavior at the CMC one may conveniently assume that, apart from the monomeric state, $N = 1$, there is only one possible micelle size, $N = \bar{N} \gg 1$. The micellar size distribution X_N then contains only two nonvanishing entries: $X_1 = \exp[(\mu - \tilde{\mu}_1^0)/k_BT]$ and $X_{\bar{N}} = \bar{N}\exp[\bar{N}(\mu - \tilde{\mu}_{\bar{N}}^0)/k_BT]$, from which the chemical potential μ can be eliminated using $X_1 + X_{\bar{N}} = X$. A numerical calculation of X_1 and $X_{\bar{N}}$ for different choices of $\bar{N}$ is shown in Fig. 1. The increased sharpness of the

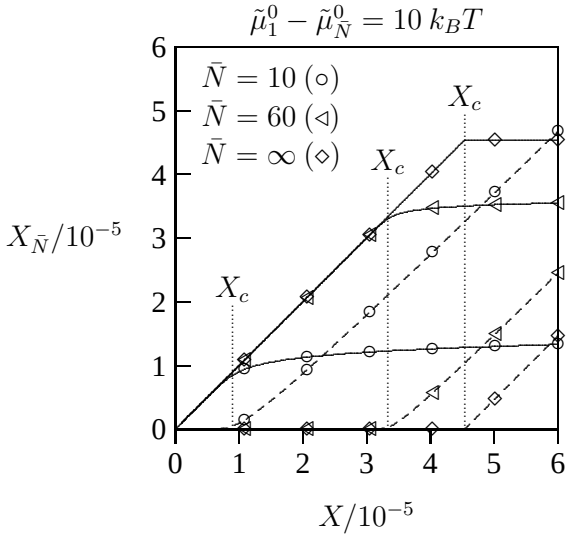

Figure 1: The mole fractions X_1 (solid curves) and $X_{\bar{N}}$ (dashed curves) as functions of the total mole fraction of amphiphiles X. The three different pairs of curves correspond to $\bar{N} = 10$, $\bar{N} = 60$ and $\bar{N} = \infty$, all for $\tilde{\mu}_1^0 - \tilde{\mu}_{\bar{N}}^0 = 10\, k_BT$. The corresponding CMC's according to Eq. 7 are $X_c = 0.9 \times 10^{-5}$ for $\bar{N} = 10$, $X_c = 3.3 \times 10^{-5}$ for $\bar{N} = 60$, and $X_c = 4.5 \times 10^{-5}$ for $\bar{N} = \infty$; they are indicated by the three vertical dotted lines.

transition for large $\bar{N}$ is apparent. As the slope of the curve describing the function $X_1(X)$ changes abruptly from X to zero, one may conveniently define the critical micelle concentration[1] X_c through $(dX_1/dX)_{X_c} =$

$1/2$. A simple calculation reveals

$$X_c = \frac{1}{\bar{N}^{\frac{1}{\bar{N}-1}}} \exp\left[-\left(\frac{\bar{N}}{\bar{N}-1}\right)\left(\frac{\tilde{\mu}_1^0 - \tilde{\mu}_{\bar{N}}^0}{k_B T}\right)\right] \approx \exp\left(-\frac{\tilde{\mu}_1^0 - \tilde{\mu}_{\bar{N}}^0}{k_B T}\right) \tag{7}$$

where the second equality is valid for $\bar{N} \gg 1$. It should be mentioned that alternative definitions for the CMC exist, either in terms of thermodynamic[16] variables or structural parameters. For example, the CMC may be defined as the concentration X for which a significant fraction (5-10%[17] or 50%[18]) of the surfactant is incorporated in micellar aggregates.

Physically, the increased sharpness of the transition with increasing $\bar{N}$ reflects the enhanced *cooperativity* of the aggregation process, approaching – in the large $\bar{N}$ limit – the behavior of a first order phase transition from monomers to a macroscopic condensed phase. (The constant monomer concentration above the CMC is then simply the solubility limit of the monomers in water.) Mathematically, the steep change in the slope of X_1 *vs* X at the CMC is evidenced by the second derivative $\left(d^2X_1/dX^2\right)_{X_c} = -\bar{N}^2$, calculated at the CMC ($X_1 = X_c$) for $\bar{N} \gg 1$. In the limit $\bar{N} \to \infty$ the system exhibit a true first order transition, see Fig. 1. Of course, since one cannot pack an infinite number of molecules in a single spherical micelles, this is a hypothetical limit for this geometry.

B. One-dimensional growth

Linear micelles are generally modeled as aggregates comprising two packing environments: a cylindrical main body and two, roughly hemi-spherical, caps at the two cylindrical ends, preventing direct contact of hydrocarbon tails with water. The micelle is often depicted as a *spherocylinder*, in which the radius of the caps is equal to the cylinder's radius, providing perfect matching between the two environments. This assumption can be relaxed, and in some cases must be modified, e.g., in systems exhibiting a second CMC, as discussed later in this chapter. However, such ramifications are mainly relevant for relatively short linear micelles. To account for the general growth characteristics of linear micelles it suffices to remember that the packing energy of amphiphiles in the end caps is different from that in the cylindrical body. The cylindrical geometry is obviously preferred over that of the caps, because otherwise there would be no thermodynamic incentive for micellar growth, (since many spherical micelles involve higher entropy than fewer longer ones). The different packing energies thus imply a positive edge energy, δ, associated with each of the two end caps. Pictorially, 2δ is the energy required for breaking a linear micelle into two shorter micelles.

Regardless of the specific structure of the end caps, the standard chemical potential $\mu_N^0 = N\tilde{\mu}_N^0$ of an N-mer can be written as

$$\mu_N^0 = N\tilde{\mu}_{cyl}^0 + 2\delta, \tag{8}$$

where $\tilde{\mu}_{cyl}^0$ is the standard chemical potential per amphiphile in the cylindrical middle part, and δ is the excess end cap energy. (Of course, $\tilde{\mu}_{cyl}^0 \ll \tilde{\mu}_1^0$.) Large end cap energy, $\delta \gg k_B T$, provides the driving force for cylindrical micelles to grow into very long, worm-like, micelles. In this case, one can safely treat N as a continuous variable, i.e., $X_N \to X(N)$, and sums over aggregate sizes can be replaced by integrals: $\sum_{N=1}^{\infty} \to \int_0^{\infty} dN$. Setting $\mu_N^0 = N\tilde{\mu}_{cyl}^0 + 2\delta$ in Eq. 3 for $X(N)$, integrating over all N and noting that $\int_0^{\infty} dN X(N) = X$, we find an explicit relationship between μ and X, i.e., $\mu = \tilde{\mu}_{cyl}^0 - k_B T/(e^{\delta/k_B T}\sqrt{X})$. Substituting this result back into into Eq. 3 then yields

$$X(N) = N \exp\left[-\frac{2\delta}{k_B T} - \frac{N}{e^{\delta/k_B T}\sqrt{X}}\right]. \tag{9}$$

We can now evaluate various properties of the micelle size distribution. For instance, the most probable aggregation number is $N^\star = e^{\delta/k_BT}\sqrt{X}$. A more common characteristic of the size distribution is the weight average of micellar sizes, $\langle N\rangle = \int_0^\infty X(N)\, N\, dN / \int_0^\infty X(N)\, dN$, for which we find the familiar result

$$\langle N\rangle = 2e^{\delta/k_BT}\sqrt{X} = 2N^\star. \tag{10}$$

For the standard deviation of the distribution we find $\sigma = \sqrt{\langle (N-\langle N\rangle)^2\rangle} = \sqrt{2}\, N^\star$, indicating a broad distribution of micellar lengths. Several examples of calculated size distributions are shown in Fig. 2.

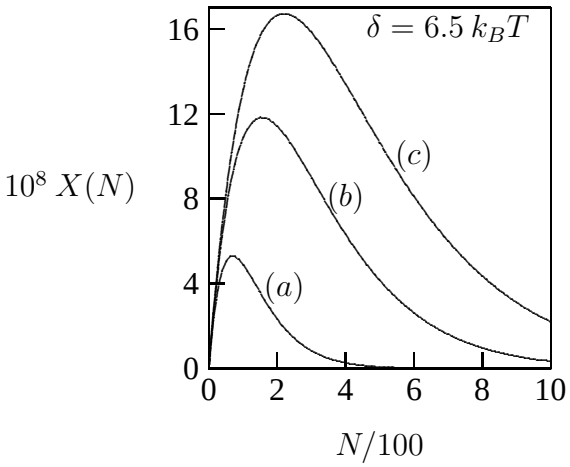

Figure 2: Size distributions, $X(N)$, of cylindrical micelles, calculated according to Eq. 9 for: (a) $X = 0.1\times10^{-4}$, (b) $X = 0.5\times10^{-4}$, and (c) $X = 1.0\times10^{-4}$. The area under each curve, $\int_0^\infty X(N)\, dN = X$, is the corresponding total mole fraction X of amphiphiles in solution. In all examples, the excess energy of a single end cap is $\delta = 6.5\, k_BT$.

Substituting $X(N)$, as given by Eq. 9 (with $\mu = \tilde{\mu}^0_{cyl} - k_BT/(e^{\delta/k_BT}\sqrt{X})$) back into the Helmholtz free energy $F[\{X(N)\}]$, (Eq. 4), we find

$$F/\mathcal{M} = X\tilde{\mu}^0_{cyl} - 2k_BT\, e^{-\delta/kT}\, \sqrt{X} \tag{11}$$

In the limit $\delta/k_BT \gg 1$ the amphiphiles strongly prefer the cylindrical packing environment, thus organizing in few very long aggregates. The only relevant contribution to the free energy in this limit is the packing energy of the molecules, namely, $F \to \mathcal{M}X\tilde{\mu}^0_{cyl}$, consistent with the last equation.

Beyond a certain length, known as the *persistence length*, ξ, which for cylindrical micelles is often on the order of several tens on nanometers (see Section IV.), the micelles behave as flexible (living) polymers. This bending flexibility is associated with an additional free energy contribution to μ^0_N which has not been included earlier. Note, however, that this contribution, which is only relevant for very long micelles, just adds to μ^0_N a linear term in N, and hence a constant term to $\mu^0_N/N \approx \tilde{\mu}^0_{cyl}$. In the phenomenological description above it may be assumed that this term is already included in $\tilde{\mu}^0_{cyl}$. Another consequence of micellar flexibility is the ability of a micelle to close upon itself into a ring, thereby eliminating the excess packing free energy, 2δ, of the end caps. However, self-closing is unfavorable for short and long cylindrical micelles. In the former case, where the micellar rod length L is considerably smaller than the persistence length, ξ, the energy required to bend the rod is generally prohibitively high. (Forming a ring by a micelle of length $L = \xi$ involves a bending energy penalty of $2\pi^2 k_BT \sim 20k_BT$). In the latter case, where $L \gg \xi$, ring closure involves a substantial loss of configurational entropy. A simple way to estimate this loss is by treating a micelle of length L and persistence length ξ, as a random walk of $L/\xi \equiv P$ steps on a 3D cubic lattice. The number of conformations available to the open micelle (ignoring self-crossing) is $\Omega_{open} = 2^{3P}$, whereas the corresponding number for the closed loop is $\Omega_{closed} = \{P!/[(P/2)!]^2\}^3$. The entropy loss upon closing the loop is thus, $\Delta S = k_B \ln[\Omega_{closed}/P\Omega_{open}]$, where the additional factor P in front of Ω_{open} accounts for the fact that the closed micelle can be broken into an open one at any of its P segments. Using

Stirling's approximation one finds $\Omega_{closed} = C\Omega_{open}\, P^{-3/2}$ where C is a constant. Hence, the free energy penalty of closing the chain, $\Delta F = -T\Delta S \approx (5/2)k_B T \ln P$, grows logarithmically with the micelle's length.

As discussed previously,[19] the entropically unfavorable reduction of the number of configurations eventually over-compensates the gain in end cap energy and thus leads to a suppression of ring-like micelles in the long micelle limit. Generally, theoretical work indicates that the conditions for ring formation are rather stringent.[20] Thus, to experimentally observe a dominating population of ring-like micelles requires – besides a large end cap energy – dilute but not too dilute conditions. It is therefore notable that In *et al*[21] have recently synthesized a tetrameric surfactant which was found to form predominantly ring-like micelles under sufficiently dilute conditions. Ring-shaped morphologies were also observed for dimeric surfactants[22]and for amphiphilic block copolymer solutions.[23]

III. Molecular packing free energy

The molecular quantity governing the micellar size distribution, $\{X(N)\}$, is the standard chemical potential, $\mu^0(N) = N\tilde{\mu}^0(N)$, of the N-aggregate. This quantity, expressing the packing free energy of the constituent amphiphiles, also dictates the relative stability of different aggregation geometries. In the three canonical packing environments – planar bilayer membranes, cylindrical micelles, and spherical micelles – the standard chemical potential per amphiphile, $\tilde{\mu}^0(N) = \{\tilde{\mu}^0_{bil}, \tilde{\mu}^0_{cyl}, \tilde{\mu}^0_{sph}\}$, depends on the geometry but not on the number of molecules in the aggregate. In these uniform environments, all molecules are equivalent, and have the same packing properties. However, many amphiphilic aggregates comprise several, or gradually varying, packing geometries. Familiar examples of more complex geometries include non-spherical globular micelles, inverted aggregates such as the inverse hexagonal phase, or pores in lipid membranes.

In this chapter we shall specifically consider several non-uniform geometries related to cylindrical micelles. These are: the curved geometry of a bent cylindrical micelle, the saddle-like structure of a tri-joint intermicellar junction, and end cap region of a rodlike micelle. In all these cases of locally varying packing geometries we may express $\tilde{\mu}^0(N)$ as an integral over all molecular contributions $\mu^0(N) = \int_{n=0}^{N} f(n)dn$, where $f(n)$ denotes the packing free energy of the nth amphiphile in the aggregate. As long as there are no long-range interactions present in the aggregate, $f(n)$ depends only on the nth amphiphile and its *local* environment. Rather than enumerating individual amphiphiles, it is more convenient to run the integration over the entire micellar (hydrocarbon-water) interface. This interface can be represented by a surface $\mathcal{S}$ (with surface element ds) that separates the hydrocarbon core of the micelle from the headgroup region. We can thus express $\mu^0(N)$ as

$$\mu^0(N) = \int_{\mathcal{S}} ds\sigma(s)f(s) \tag{12}$$

where $\sigma(s)$ is the local surface density of headgroups around point s on $\mathcal{S}$. The local free energy $f(s)$ is a function of the position s on $\mathcal{S}$. The aggregation number corresponding of the N-mer in Eq. 12 is given by $N = \int_{\mathcal{S}} ds\sigma(s)$.

A. Free energy contributions

There are three major contributions to the average packing free energy per molecule, f, of an amphiphilic molecule in a self-assembled aggregate: (i) f_h – the headgroup, or more precisely inter-headgroup in-

teraction free energy, (ii) f_s – the interfacial energy associated with the (small) contact area (a) between the hydrocarbon tails and the surrounding aqueous solution, and (iii) f_c – the packing free energy of the hydrophobic tail. A common assumption in modeling the energetics of micellar aggregates is to ignore additional contributions to f and treat this function as a sum of the above three terms, $f = f_h + f_s + f_c$, for any point on $\mathcal{S}$. All three contributions may depend on the local geometry; i.e., on the local cross-sectional area per molecule $a = a(s) = 1/\sigma(s)$ and on the local interfacial (principal) curvatures c_1 and c_2. The additivity of f is a most reasonable approximation, in view of the fact that the hydrophobic effect[1,13,17] creates a robust interfacial region which physically separates the headgroups from the tails. Hence, headgroup interactions, which include steric as well as electrostatic interactions between them may sensitively depend on the local a, c_1, c_2, but are independent of the structure and conformational statistics of the tails.

The opposing forces model (OFM) mentioned in Section I., has been suggested by Israelachvili *et al* to account for the thermodynamic stability of micelles, membranes and other self-assembled amphiphilic aggregates.[13,14,18] This phenomenological model proposes simple expressions for both the interfacial and headgroup energies, namely, $f_s = \gamma a$ and $f_h = B/a$. The first expression ($f_s = \gamma a$) accounts for the unfavorable contact energy between water molecules and hydrocarbon chain segments at the interface between the hydrophobic core and the surrounding solution. Thus γ is the effective surface tension corresponding to this interface, which is often approximated by the water-alkane surface tension $\gamma \approx 50\ erg/\text{Å}^2 = 0.12\ k_BT/\text{Å}^2$. The second term, $f_h = B/a$, is a phenomenological expression which lumps all headgroup interactions in a single parameter B. Because inter-headgroup forces are generally repulsive and thus tend to increase a, $f_h = B/a$ may be regarded as the first order term in the expansion of f_h in powers of $1/a$.

In its simplest form the OFM assumes that both the interfacial and headgroup forces act within the same interaction surface, commonly regarded as located at the hydrocarbon-water interface. A simple extension of the model assigns to the headgroups their own interaction plane, at distance l_h away from this interface. The headgroup contribution to f is then given by $f_h = B/a_h$, where the cross-sectional area per headgroup $a_h = a[1 + (c_1 + c_2)l_h + c_1c_2l_h^2]$ is related to a through the two principal curvatures, c_1 and c_2, of the interface $\mathcal{S}$. The two forces, interfacial tension and headgroup repulsion act in opposite directions, attempting, respectively, to minimize and maximize a, the interfacial area per molecule. They balance each other (i.e., minimize $f_s + f_h$) at the "optimal" headgroup area $a = a_0 = (B/\gamma)^{1/2}$. The free energy per amphiphile can thus be expressed in the form

$$f = \gamma a\Big(1 - \frac{a_0}{a}\Big)^2 + f_c \tag{13}$$

Another major assumption made in most applications of the OFM is that f_c, the chain contribution to the molecular packing free energy, is a constant, independent of the aggregation geometry. This model thus suggests that amphiphiles always tend to pack into aggregates enabling $a = a_0$. More precisely, the model predicts that, for entropic reasons, amphiphiles in solution will preferentially assemble into the smallest aggregates allowing $a = a_0$. Underlying the assumption $f_c = constant$ is the notion that the hydrophobic core of amphiphilic aggregates is liquid-like, i.e., uniformly packed with hydrocarbon chain segments, at the density of a liquid phase of such chains. While this notion, known also as the *hydrocarbon droplet assumption*,[13,14] is supported by both experiment and theory, it does not mean that the conformational statistics of the tails, and hence f_c, are not affected by changes in the packing geometry of the chains. In fact, in the next section we shall employ the assumption that the hydrophobic region is a liquid-like core as a constraint on the probability distribution of chain conformation, thus deriving its dependence on the geometry of the packing environment. It should nevertheless be noted that the simple OFM (with $f_c = constant$) provides a convincing qualitative explanation for the preference of specific amphiphiles to

aggregate into spheres, cylinders or other structures. Still, as mentioned already in Section I., in itself, it cannot reasonably account for such properties like the curvature elasticity of lipid bilayers[15] or, as we shall see below, for the bending rigidity of cylindrical micelles. For these properties it is imperative to take into account both the interfacial ($f_s + f_h$) and chain (f_c) contributions to f.

In the next section we briefly outline a mean-field theory of chain packing in micellar aggregates. The theory has been widely applied for the calculation of thermodynamic functions (e.g., packing free energies, bending rigidities) and structural properties (e.g., bond orientational order parameters of amphiphile chains in bilayers and micelles), showing generally very good agreement with experimental and computer simulation data.[15,24]

B. Chain conformational statistics

A single hydrocarbon chain immersed in an aqueous solution perturbs the structure of water around it, resulting in unfavorable, "hydrophobic", interactions between chain segments and water molecules. The area of hydrocarbon-water contact is reduced when the chains condense to form a hydrocarbon droplet, such as the inner core of a micelle. This *hydrophobic effect*[17] constitutes the main driving force for amphiphile assembly into compact structures. Upon condensing into a liquid-like core each chain gains a certain cohesive (i.e., negative) energy, g, which depends on the segment density but not on the geometry of the aggregate. Assuming that this density is independent of the size and curvature of the hydrophobic core, one can safely assume that g provides a constant contribution to f_c, which for convenience may be set equal to zero. On the other hand, the conformational statistics, and hence the internal free energy, of the chains may be strongly affected by the packing geometry. The local packing geometry of a chain is fully specified by the area per molecule a, and the two principal curvatures c_1, c_2 of the hydrocarbon-water interface, implying $f_c = f_c(a, c_1, c_2)$. Below we outline a rather simple theoretical approach for calculating f_c.

The central quantity in this mean-field approach[15,25,26] is the probability distribution function (pdf), $P(\alpha)$, describing the probability of finding the chain in a given conformation, α. $P(\alpha, s)$ depends generally on the local packing geometry at point s on $\mathcal{S}$, as specified by the local a, c_1, c_2. In non-uniform, rapidly varying, packing geometries (e.g., of lipid molecules around an integral membrane protein) the calculation of $P(\alpha, s)$ is quite complicated, and depends also on the local environment s' at which *neighboring* chain originate.[27,28] Here, for brevity, we shall briefly outline the theory and only for a uniform aggregate geometry.

The local conformational free energy per chain is given by

$$f_c = u_c - Ts_c = \sum_\alpha P(\alpha)\epsilon(\alpha) + k_B T \sum_\alpha P(\alpha) \ln P(\alpha) \tag{14}$$

where the summations run over all accessible chain conformations α. The energetic contribution u_c represents the conformational average over the internal energy $\epsilon(\alpha)$ associated with each individual conformation α. For simple, saturated alkyl hydrocarbon tails, for instance, the $\epsilon(\alpha)$'s are determined by the trans/gauche bond sequence along the chain. The second sum in Eq. 14 is the conformational entropy of the chain.

The equilibrium pdf, $P(\alpha)$, is found by minimizing f_c in Eq. 14 subject to the normalization condition $\sum_\alpha P(\alpha) = 1$ and subject to the relevant geometric packing constraints. These constraints express the average shape that the chain must adopt in order to fit into a specific aggregate geometry. The constraint can be formulated as

$$\sum_\alpha P(\alpha)\varphi(\alpha, z) = a(z) = a(z/b)^{2-d} \quad ; \quad 0 \le z \le b \tag{15}$$

where $\varphi(\alpha, z)dz$ is the volume occupied by a chain in conformation α within a shell $z, z + dz$, parallel to the interface $\mathcal{S}$ of the micelle; $a(z)$ denotes the area available per chain at position z. The second equality in Eq. 15 specifies $a(z)$ for the three canonical packing geometries, with $d = 0, 1, 2$ denoting the growth dimensionalities of spherical, cylindrical and planar bilayer aggregates, respectively. Here a is the cross-sectional area of the chain at $\mathcal{S}$ and b is the thickness of the hydrocarbon core. Note that $ab/(3-d) = \nu$ is the (constant) volume ν of the hydrocarbon chain in the liquid-like core. The conditional minimization of $F[\{P(\alpha)\}]$ yields

$$P(\alpha) = \frac{1}{q} \exp\left\{ -\left[\epsilon(\alpha) + \int_0^b dz\, \pi(z)\phi(\alpha, z) \right] / k_B T \right\} \tag{16}$$

where the partition function q ensures the normalization of the equilibrium pdf, and where $\pi(z)$ is the lateral pressure profile that emerges as the set of Lagrangian multipliers conjugate to the packing constraints, Eq. 15. Physically, $\pi(z)$, represents the lateral pressure imposed on an otherwise free (isolated) chain in order to fit into the volume available to it in the compact aggregate.

Substituting $P(\alpha)$ from Eq. 16 back into the packing constraint, Eq. 15, we obtain – as is often the case in mean-field theories – a self-consistency relation for the pdf; here a coupled set of equations for the $\{\pi(z)\}$. Any actual calculation of the lateral pressure profile must be based on the appropriate molecular chain model. An adequate representation of saturated alkyl (polymethylene) chains, for example, is provided by the *rotational isomeric state model*.[29] Its input parameters are the geometrical characteristics of the chain, i.e., the C-C bond length, methylene segment size, bond angles, and the trans/gauche isomerization energy. After evaluating the $\pi(z)$, and hence the equilibrium pdf, we can use Eq 14 in order to calculate f_c. The results of such numerical calculations for $-(CH_2)_{13}CH_3$ (C-14) chains, packed in the three basic geometries, are shown in Fig. 3 as a function of the aggregate's half thickness b. Note that the maximal

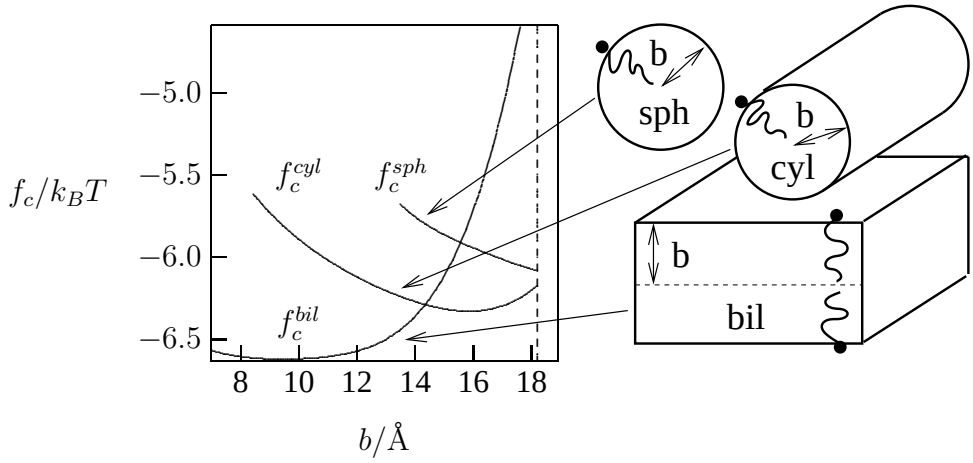

Figure 3: Chain conformational free energy in the three canonical geometries (sphere, cylinder, and planar bilayer – schematically displayed on the right hand side of the diagram) as a function of the hydrophobic half-thickness b. The calculations are for $-(CH_2)_{13}CH_3$ (C-14) tails, whose chain volume is $\nu = 405$ Å^3. The dashed line denotes the length $b_{max} \approx 18$ Å of a maximally stretched (all-trans) chain, beyond which f_c increases drastically. The minimum of f_c^{sph} is achieved very close to that length. Adapted from May *et al*[30] with permission.

chain length for C-14 is $b_{max} \approx 18$ Å, beyond which f_c would increase extremely steeply since $b > b_{max}$

implies the appearance of (a highly unfavorable) void space inside the hydrocarbon core. Interestingly, the minimum of f_c appears at very different thicknesses b for the different geometries: $b = 10$ Å, 16 Å, and 18 Å. These values correspond to the interfacial areas per molecules: $a = 40$ Å^2, 51 Å^2, and 68 Å^2, for the bilayer, cylinder, and sphere, respectively. It should be stresses that even though the changes in f_c for different b's are only fractions of k_BT for individual molecules, they can amount to substantial free energy difference for a whole micelle.

C. Micellar stability

In this section we consider the implications of Eq. 13 with respect to the stability of the three canonical aggregation geometries. It is instructive to first consider the predictions of the simple OFM model in which, as discussed above, f_c is treated as a constant,[13] (which for simplicity may be set equal to zero). Ignoring f_c, the OFM predicts a most stable aggregate if $a = a_0$, implying $f = 0$. In general there will be more than one packing geometry enabling $a = a_0$, in which case the preferred micellar geometry is the one which corresponds to the smallest possible (hence maximally curved) aggregate, because many small aggregates carry more translational entropy than fewer larger ones. To quantify this notion it is common to define the *packing parameter* $P = \nu/(a_0 b_{max})$, where, as before, ν is the chain volume, and b_{max} is the length of the maximally extended tail. For minimal packing energy we require $a = a_0$ as well as $b \leq b_{max}$ in order to ensure a compact hydrophobic core. Noting that $\nu/a_0 b = 1/3, 1/2$ and 1, for spheres, cylinders and planar bilayers, respectively, it follows that $P \leq 1/3$ allows optimal packing in all three geometries. As argued above, however, spherical micelles will be preferred on entropic grounds. Similarly, $1/3 < P \leq 1/2$ allows both cylinders and bilayers, but cylinders are preferred because of their higher curvature. Bilayers prevail when $1/2 < P \leq 1$, and inverted structures for $P > 1$.

Let us now calculate f, including the chain conformational free energy f_c. We calculate the optimal aggregate half-thickness $b = (3-d)\nu/a$ and the corresponding free energy f as a function of the headgroup repulsion strength B for the three canonical aggregate geometries: bilayer (bil, $d = 2$), cylinder (cyl, $d = 1$), and sphere (sph, $d = 0$). Fig. 4 shows the numerical results for C-14 chains, using the values of f_c shown in Fig. 3. (To get a feeling for the order of magnitude of B values, recall that $B = \gamma a_0^2$, so that for, say, $\gamma = 0.12\ k_BT/$Å^2 and $a_0 = 50$ Å^2 we obtain $B = 300\ k_BT$Å^2.) The quantities plotted in the left diagram are the free energy differences, $\triangle f_{bil} = f_{bil} - f_{cyl}$ and $\triangle f_{sph} = f_{sph} - f_{cyl}$ of, respectively, the bilayer and sphere compared to the cylindrical structure. The signs of $\triangle f_{bil}$ and $\triangle f_{sph}$ suggest that as B increases the stable aggregation structure undergoes – as expected – the sequence: planar $\rightarrow$ cylindrical $\rightarrow$ spherical. The corresponding equilibrium half-thicknesses, b, are shown in the right diagram (solid lines); the prediction from the OFM (with $f_c = 0$) are also displayed (dashed lines). In all cases, an increase in the headgroup repulsion strength, B, tends to increase a and thus lower b. The crossing points of the corresponding solid and dashed lines in the right diagram indicate the location of the minima of $f_c(b)$ (see Fig. 3). The close correspondence of the two models argues that the aggregate thickness, b, and thus the cross-sectional area a, is indeed mainly determined by headgroup interactions.

IV. Bending elasticity of cylindrical micelles

Short cylindrical micelles, whose length is just a few times larger than their diameter are reasonably described as rigid rods. On longer length scales the micelles exhibit non-negligible bending fluctuations along their contour, and their conformational statistics conform to the *worm-like chain*, or *persistent polymer*,

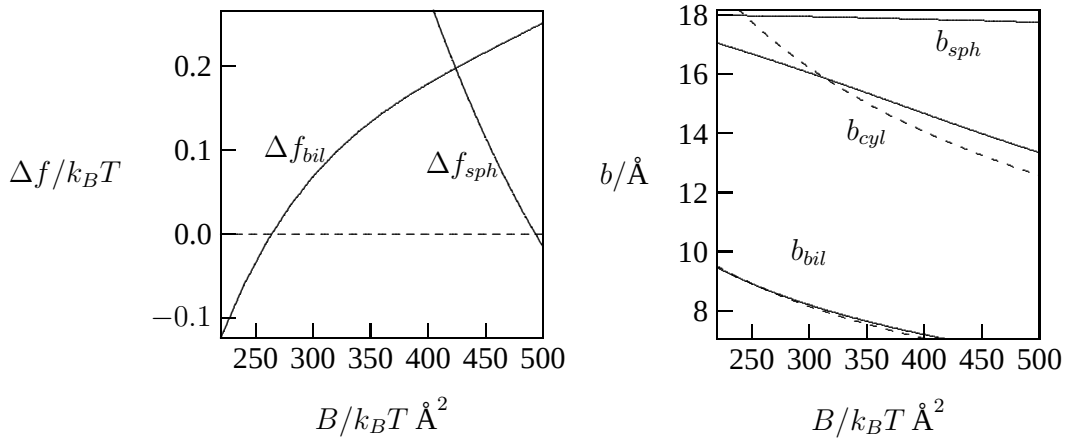

Figure 4: The difference in the free energy per molecule between a planar bilayer and a cylinder ($\triangle f_{bil} = f_{bil} - f_{cyl}$), and between a sphere and a cylinder ($\triangle f_{sph} = f_{sph} - f_{cyl}$) (left), as a function of the headgroup repulsion strength B. Also shown is is the aggregate thickness b (right, solid lines) for which f is minimal. The dashed lines correspond to the optimal b, as implied by the requirement for optimal headgroup area ($a = a_0$), ignoring the tail contribution f_c. In this calculation, a small distance of $l_h = 1$ Å was assumed to separate between the hydrocarbon-water and headgroup interaction surfaces. Adapted from May *et al*[30] with permission.

model.[31,32] In this model, which is also adequate for describing thermal orientational fluctuations of relatively stiff biopolymers such as DNA or actin, the polymer is depicted as an homogeneous elastic filament undergoing moderate ("harmonic") bending deformations. Thus, the energetic cost $\triangle F$ associated with the uniform bending of (a section of) a cylindrical micelle of length L is,

$$\frac{\triangle F}{L} = \frac{1}{2}\kappa c^2 = \frac{1}{2}k_BT\xi c^2 \tag{17}$$

where c is the curvature of the deformation, κ is the 1D bending modulus, and ξ is the *persistence length* of the micelle in question. The persistence length measures the length of angular correlations along the micelle's contour, namely, $\langle \cos\theta \rangle = \exp(-s/\xi)$, where s is the contour length between two points on the micelle's axis, and θ is the angle between the chain (tangential) directions at these points. For small curvature deformations this yields $\langle c^2 \rangle = 2s/\xi$. On the other hand, from the first equality in Eq. 17 it follows (by Boltzmann averaging) that $\langle c^2 \rangle = 2sk_BT/\kappa$, explaining the relationship $\xi = \kappa/k_BT$ expressed by the second equality in this equation.[31] Consider now a segment of the micelle of length (say) $L = 2\xi$, and suppose it is uniformly bent to an arc of radius $c \sim 1/\xi$, implying a substantial change of directions, $\theta \approx 120^o$, between the two ends of this segment. From Eq. 17, the energetic cost of angular fluctuations of this order of magnitude is small,$\sim k_BT$. Such fluctuations are thus highly probable, consistent with the interpretation of ξ as the decay length of angular correlation along a worm-like chain. This also means that a long, worm-like, micelle of length L can be regarded as a freely jointed polymer composed of $L\xi$ (Kuhn) segments[31,32] of length ξ. The mean end-to-end distance of the micelle is thus $\sqrt{R^2} = \xi\sqrt{(L/\xi)} = \sqrt{(\xi\, L)}$.

Upon bending a micelle, the flexible tails comprising the hydrocarbon core can easily readjust their chain conformations, thus relieving much of the curvature stress. Similarly, possibly on a somewhat longer time scale, the polar headgroups can rearrange their positions on the micellar surface thus also lowering the deformation energy penalty. This ability to accommodate the curvature stress, while maintaining the

micelle's integrity, reflects the relatively "soft" internal degrees of freedom of self-assembled amphiphilic aggregates, as compared to stiffer, semiflexible[32] filaments, which are governed by stronger cohesive forces, such as double stranded DNA, F-actin or microtubules. The bending rigidity κ of a worm-like micelle is thus expected to be smaller than that of a comparably thick semiflexible filament. Indeed, bending constants of cylindrical micelles are typically in the range $\kappa = \xi\, k_BT = (100 \cdots \ldots 500)\, k_BT$Å, smaller than that of dsDNA for example ($\kappa \approx 600\, k_BT$Å for B-DNA). This difference is more significant considering that the radius, $b = 10$ Å, of the DNA rod is considerably smaller than typical micellar radii, e.g., $b = 16$ Å for C-14 micelles, see Fig. 4. More explicitly, homogeneous rod-like materials can be characterized by $\kappa = (\pi/4)Yb^4$, where b is the radius and Y is Young's modulus with a typical value of $Y = 0.5 \times 10^9\ J/m^3$ for biomaterials.[33] This, indeed, roughly recovers the bending stiffness of B-DNA ($\kappa = (\pi/4)Yb^4 = 950 k_BT$Å for $b = 10$ Å). but yields $\kappa = 6000 k_BT$Å for a $b = 16$ Å rod, much larger than the bending rigidity of a similarly thick micelle.

A better estimate of the bending rigidity of cylindrical micelles may be obtained based on the 2D elastic properties of other soft aggregates, especially 2D lipid bilayers or surfactant monolayers, whose curvature elasticity has been extensively studied for many systems using diverse techniques.[34] The elastic deformation energy, $\triangle F$, associated with the (uniform) bending of such a layer of area A, to principal curvatures c_1 and c_2 is given by[35]

$$\frac{\triangle F}{A} = \frac{1}{2}K(c_1 + c_2 - c_0)^2 + \bar{K}c_1c_2 - F_{eq} \tag{18}$$

Here K and $\bar{K}$, are the splay and saddle-splay moduli, respectively, and c_0 is known as the spontaneous curvature. $F_{eq} = c_0^2\bar{K}K/(2\bar{K} + 4K)$ is the free energy in the equilibrium state, in which case $c_1 = c_2 = c_{eq} = c_0\, K/(2K + \bar{K})$. Even though Eq. 18 is strictly valid only for small curvatures, we may use it to estimate the 1D bending stiffness of a cylindrical micelle. To this end we treat the straight cylindrical micelle of length L and radius b as a (closed) circular monolayer of surface area $A = 2\pi bL$, bent so that $c_1 = 1/b$, $c_2 = 0$. Furthermore, we regard the micelle as composed of two semi-cylinders, each of area πbL, so that upon bending along its main axis it appears as a section of a torus. The "outer" half of the torus is convex, with $c_2 = c > 0$, while the inner one is concave, with $c_2 = -c < 0$; $c_1 = 1/b$ is unchanged. Using Eq. 18 for this model it is easily shown that up to quadratic order in curvature $\triangle F = L\pi bKc^2/2$, and hence the simple relationship $\kappa = \pi bK$, independent of c_0 and $\bar{K}$, between the 1D and 2D bending constants emerges.[30] As the splay modulus of surfactant monolayers is typically $K \sim 10\, k_BT$, the prediction for the 1D bending stiffness of the cylindrical micelle is $\kappa = 320\, k_BT$Å. A very similar estimate would follow by considering the 1D bending (i.e., to $c_1 = 0, c_2 = c$ of a strip of a planar ($c_1 = c_2 = c_0 = 0$) bilayer of length L and width $\sim b$. Noting the additive contribution from the two bilayer leaflets one finds now $\kappa = 2Kb$. Simple dimensional analysis also suggests $\kappa \sim bK$. A comparison of this relation with measured values of κ and K for SDS micelles was recently made by Magid *et al.*[36]

A closer insight into the mechanism underlying the bending elasticity of cylindrical micelles may be gained using the simple molecular-level model, Eq. 13. First we note that in a straight cylindrical micelle, all chains are directed, on average, towards the axis of symmetry, located exactly at the center of the rod. It is reasonable to assume that upon bending the tails will still point towards a common axis which, however, need no longer coincide with the mid-axis of the micelle. It may be shifted by a distance ϵb towards the bending (concave) direction as depicted in Fig. 5. The shift ϵ is dictated by the balance between two, generally competing, tendencies. One of these, as expressed by the first term in Eq. 13, is the tendency to maintain the surface area per molecule a, equal to the optimal value, a_0, as implied by the OFM. Since the overall area-to-volume ratio of a cylinder does not change upon bending, there is no change in the *average* surface area per molecule. Thus assuming (consistent with the simple OFM) that changes in f_c during bending are negligible, we would conclude $\kappa \equiv 0$. For the molecular packing model depicted in Fig. 5 it

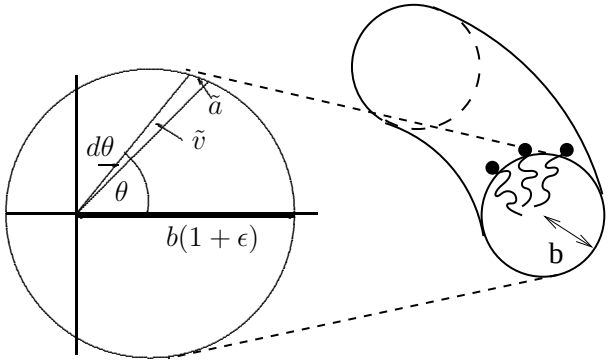

Figure 5: Schematic representation of a homogeneously bent cylindrical micelle, of radius b, forming a section of a torus. The zoom into its interior specifies the common axis towards which the tails of all amphiphiles are directed on average. This axis is located at distance ϵb away from the mid-axis. The local area and volume elements at angle θ are $da = \tilde{a}d\theta$ and $dv = \tilde{a}d\theta$, respectively.

can be shown that $a = a_0$ is achieved for $\epsilon = cb/3$.[30]

Unlike the inerfacial forces which act towards $a = a_0$ (and hence $\epsilon = cb/3$) the chain conformational free energy, f_c, tends to keep $\epsilon = 0$. The balance of these tendencies will yield $0 < \epsilon < cb/3$. To determine the dependence of ϵ on c it is convenient to use the linear form $\epsilon = \eta c$ and determine the optimal *relaxation parameter* η by minimizing the bending deformation energy. Referring to Fig. 5, let $l(\theta)$ denote the effective tail length of a molecule anchored at angular position θ. The corresponding cross-sectional area per molecule $a(\theta) = \nu\tilde{a}/\tilde{v}$ can be calculated using appropriate parameterization of the local area and volume elements, $dA = \tilde{a}d\theta$ and $dV = \tilde{v}d\theta$.[37]

For a given η, calculating the 1D bending stiffness based only on the OFM contribution to the bending energy (i.e., setting $f_c = 0$ and $f = \gamma a(1 - a_0/a)^2$)) one finds[30]

$$\kappa_h = (2/9)b\gamma\pi\,(b - 3\eta)^2 \tag{19}$$

where $a = a_0 = 2\nu/b$ was used here for the straight cylinder. This is the OFM contribution to the 1D bending modulus $\kappa = \kappa_h + \kappa_c$ which, as noted above, yields $\kappa_h = 0$ for $\eta = \eta_h = bc/3$ (corresponding to $a(\theta) = a_0$ for all chains).

Clearly, however, if the straight cylinder offers optimal packing conditions for the hydrocarbon tails, they would prefer $l(\theta) \equiv b$ for all chains, implying $\eta = \eta_c = 0$. The optimal η should thus be determined by minimizing the sum of head and tail contributions. The chain conformational energy can be calculated numerically using the chain packing theory outlined in Section III.B., (see below), or estimated using an approximate closed form expression for f_c. A reasonable approximate representation of $f_c(\theta)$ is provided by the quadratic form

$$f_c(\theta) = \tau\gamma a_0\,(1 - l(\theta)/b^\star)^2 \tag{20}$$

which appears consistent with numerical calculations of chain energies, such as those shown in Fig. 3. Here $b^\star$ is the optimal tail length of a chain packed in a cylindrical geometry, and the dimensionless coefficient τ measures the resistance of the chain to deviations from $b^\star$. For the C-14 with $B = 300\,k_BT$ Å^2, Figs. 3 and 4 suggest that $b^\star$ is actually equal to the radius $b = 2\nu/a_0$ of the straight cylindrical micelle. Based on the last equation it can be shown[30,37] that

$$\kappa_c = 2\pi b\gamma\tau\,\eta^2 \tag{21}$$

where for simplicity we have set $b^\star = b$. Minimizing $\kappa(\eta) = \kappa_h + \kappa_c$, using Eqs. 19 and 21, one finds that the optimal η and κ are given by

$$\eta = \frac{b}{3(1+\tau)}, \qquad \kappa = \frac{2}{9}\,\gamma\,\pi\,b^3\,\frac{\tau}{(1+\tau)}, \tag{22}$$

It may be noted that in addition to chain stretching f_c may include a contribution due to tilt deformation. Tilt refers to the deviation of the average chain direction from the normal direction of the polar-apolar interface. The tilt deformation of amphiphilic layers has received some interest in recent years, particularly for lipid membranes[38–41] but its consequences with respect to the energetics of cylindrical micelles have not been studied so far.

Rather than using the phenomenological expression in Eq. 20, the function $f_c(c)$ can be computed based on the formalism described in Section III.B.. Such a calculation has been performed for an approximate model of the bent cylindrical micelle,[30] according to which the cylinder is divided into an an external (convex) and an internal (concave) region, as shown in the inset in Fig. 6. Assuming that all chains in each of the two regions are equally distorted, the contribution κ_c was calculated based on a numerically performed curvature expansion. As a concrete example, the inset in Fig. 6 shows the average conformational free energies of a chain in the external (E) and internal (I) parts of a bent cylindrical micelle with curvature $c = 1/90\,\text{Å}$. This figure also shows that the chain packing energy in the straight cylinder is always intermediate between those of the internal and external regions (dashed curve). The calculated dependence of κ_c on η for $B = 300\ k_BT\text{Å}^2$ (and thus $b = 16$ Å) is shown in Fig. 6. Also shown is κ_h, as derived from the OFM. The overall bending stiffness, $\kappa = \kappa_h + \kappa_c$, adopts its minimum $\kappa = 160\ k_BT\text{Å}$ at $\eta = 3.5$. These

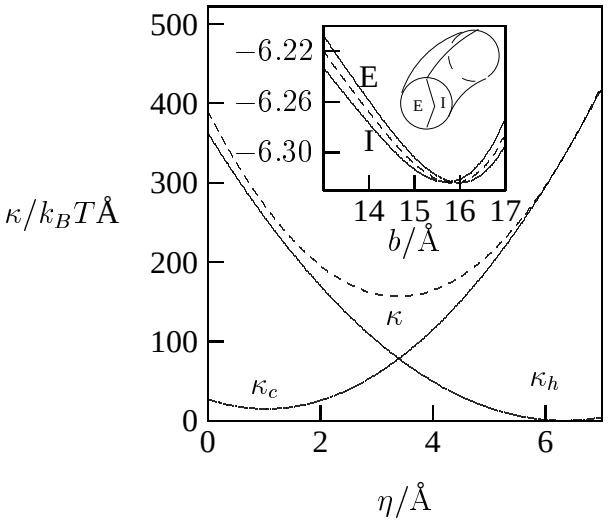

Figure 6: The bending modulus κ and its components κ_c and κ_h (all in units of k_BT Å) as a function of the relaxation parameter η for $B = 300\ k_BT\ \text{Å}^2$. Optimal relaxation is found for $\eta \approx 3$Å. The inset shows the average conformational free energy f_c in units of k_BT in the external (convex, E) and internal parts (concave, I) of a bent cylindrical micelle with $c = 1/90\,\text{Å}$. The dashed line is f_c for a straight micelle with $c = 0$. Adapted from May *et al*[30] with permission.

estimates compare well with the predictions of the phenomenological model according to Eq. 22: $\eta = 2.7$ and $\kappa = 170\ k_BT\text{Å}$ for $\tau = 1$ and $b = 16$ Å.

The scaling of the persistence length $\xi \sim b_{max}^{\alpha}$ with the length b_{max} of the surfactant tails has been investigated theoretically on the basis of a self-consistent field theory by Lauw *et al*;[42] the predicted exponent was $\alpha = 2.4 - 2.9$. This is slightly smaller than $\alpha = 3$, predicted by Eq. 22 (under the assumption that τ is independent of chain length).

The persistence length ξ has been determined for a large number of cylindrical micelles. Rough estimates can be obtained using light scattering methods[43,44] or microscopic imaging such as Cryo-TEM[21] or AFM.[45] Precise measurements[6,36,46,47] are based on small-angle neutron scattering which yields high-resolution scattering functions that can be compared with theoretical predictions. In fact, owing to the complexity in the behavior of worm-like micellar solutions, Monte-Carlo simulations have proven to be the most appropriate tool to simulate these scattering functions.[46,48]

V. The sphere-to-rod transition and the second CMC

The minimal micelles formed at the CMC, even those that quickly elongate into worm-like micelles, are almost invariably spherical. If the optimal packing radius in the elongated cylindrical body were equal to that of the minimal spherical micelles, all micelles would grow as perfect sphero-cylinders. For this model the standard chemical potential (i.e., the amphiphile packing free energy) of the micelle is a simple sum of contributions from molecules packed in the spherical body and the two hemi-spherical caps: $\mu_N^0 = N\tilde{\mu}_{cyl}^0 + 2\delta$, with $\delta = (\bar{N}/2)(\tilde{\mu}_{sph}^0 - \tilde{\mu}_{cyl}^0)$ for $N \geq \bar{N}$; $\bar{N}$ denoting the number of molecules in the minimal micelle. According to this model micellar growth, or is it is often called - the *sphere-to-rod transition* – is a continuous process, with the average micellar size increasing monotonically as a function of X (scaling with $\sqrt{X}$ at higher concentrations), as illustrated in Fig. 2. Experimentally, however, it is often observed that the sphere-to-rod transition is discontinous. That is, a second critical concentration, X_{2c}, must to be surpassed in order to initiate the growth from globular into cylindrical micelles. X_{2c} marks the total amphiphile concentration at the onset of cylindrical growth. Between the two critical concentrations, X_c and X_{2c}, added amphiphiles merely increase the number of globular micelles without transforming them into elongated aggregates.

The first experimental evidence for this peculiar behavior was reported for cetylpyridinium bromide (CPBr) by Porte *et al*[49] who also introduced the term "second CMC" for X_{2c}. Meanwhile, a second CMC has been observed for various other amphiphiles, including cationic dimeric (gemini)[22,50] and nonionic[51,52] amphiphiles, as well as various alkylpyridinium salts.[53] Cryo-TEM images indicate two distinct micellar populations above the second CMC[22,51] : globular and cylindrical. The cylindrical micelles appear to be semiflexible and with spherical end caps. Notably, both the globular micelles and the micellar end caps have larger diameters than the cylindrical main body. For diblock copolymers that self-assemble into worm-like micelles this feature is even more pronounced, as seen in cryo-TEM images.[54,55] Small cylindrical micelles, with mid-sections comparable to the size of the end caps, are generally not observed.

What then is the reason for the experimentally observed *discontinous* transition from globular to elongated micelles? The presence of two distinct micellar populations clearly suggests that the packing properties of short cylindrical aggregates are energetically unfavorable. Their appearance is thus suppressed, resulting in a discontinous transition from spherical to long cylindrical aggregates. This basic notion underlies previous theoretical models of the second CMC,[56–58] and is also consistent with a recent simulation study.[59]

The suppression of short cylindrical micelles can be viewed as the result of an energetically unfavorable "repulsion" between the two (partly) spherical end caps. For non-ionic amphiphiles this repulsion is likely a result of elastic interactions through the cylindrical main body, as illustrated in Fig. 7. For charged micelles, long-range electrostatic interactions may induce similar effects as will be discussed in Section VII..

Amphiphiles residing within the spherical end caps are subject to the spherical packing geometry, whereas those in the cylindrical main body experience cylindrical packing conditions. If the cross-sectional area per headgroup in both packing geometries were exactly the same, then the radius b_{sph} of the end cap would be larger than the radius b_{cyl} of the cylindrical main body by a factor of $3/2$. On the other hand, assuming size-matching ($b_{sph} = b_{cyl}$) between end cap and cylindrical main body (as for a perfect sphero-cylinder) the area per headgroup within the end caps must increase to $a_{sph} = 3a_{cyl}/2 = 3\nu/b_{cyl}$, where ν is the amphiphile's tail volume and a_{cyl} is the cross-sectional headgroup area within the cylindrical main body. Based on the OFM (see Eq. 13) we then obtain an excess end cap energy of $\delta = 2\pi\gamma b_{cyl}^2/9$, which amounts to more than $20\ k_BT$ for $b_{cyl} = 16$ Å. The energetic incentive to minimize the excess end cap energy by increasing b_{sph} beyond b_{cyl} is thus substantial.

Geometrically, a structure composed of a cylindrical body of radius b_{cyl}, capped by two truncated spher-

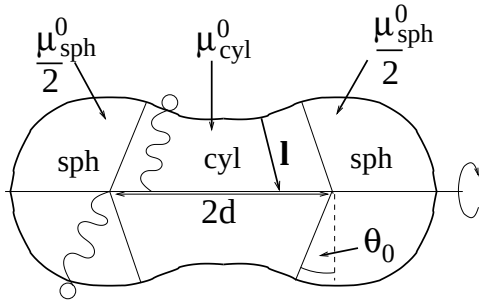

Figure 7: Illustration of a cross section along the axis of symmetry of a short cylindrical micelle with two end caps (denoted by "sph" and separated by distance $2d$). Each end cap induces an elastic (chain packing) perturbation within the cylindrical main body (denoted by "cyl"). Overlap of the perturbations results in effective repulsion between the two ends. The perturbation can be characterized by a position-dependent vector $\mathbf{l}(\mathbf{r})$ that specifies the length ($l = |\mathbf{l}|$) and orientation of the amphiphiles. The overall packing free energy $\mu^0 = \mu^0_{sph} + \mu^0_{cyl}$ is the sum of contributions from the two end caps (μ^0_{sph}) and from the cylindrical main body (μ^0_{cyl}). Adapted from May and Ben-Shaul[56] with permission.

ical end caps (as in Fig. 7) of a larger radius is not impossible. However, chain packing considerations imply that a micelle of this geometry is quite unlikely to form. First, the chains cannot be stretched beyond their maximum length. In Fig. 3 we see that, e.g., for C-14 chains, the minimal chain packing energy in the cylindrical geometry is achieved for $b_{cyl} = 16$ Å. Assuming that this is also the micellar radius preferred by the headgroups, then to ensure the same area per headgroup in the end caps their spherical radius should be $b_{sph} = (3/2)b_{cyl} = 24$ Å, much larger than the length of a fully extended chain, which is 18 Å. Thus, $b_{sph} = b_{max} = 18$Å (which also corresponds to the minimum chain packing energy in a sphere) is the largest end cap radius for the C-14 chains. According to the OFM, the corresponding energetic difference between a spherical end cap of $b_{sph} = 18$ Å compared to $b_{sph} = b_{cyl} = 16$ Å is still considerable; $\delta = 15\, k_B T$.

Another important chain packing consideration involves the transition zone between the end caps and the cylindrical main body. The chain stiffness (together with the OFM) defines a length scale that determines the spatial relaxation of aggregate thickness from the end caps towards the cylindrical main body. Typically, this length scale is comparable to the micellar thickness, thus being of the order of a few nm for most amphiphiles. The shape of the transition zone may be adjusted by the micelle so as to minimize its free energy. Recent modeling attempts have used various structural assumptions, such as conical[30] or catenoidal[57] transition zones, while others have calculated the shape of the transition region through functional minimization.[56] An example for the structure of a cylindrical micelle as calculated by functional minimization is shown in Fig. 8. As can be seen, the presence of the hemi-spherical end cap induces a

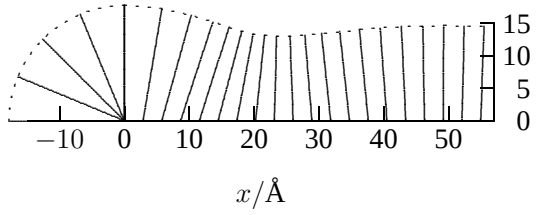

Figure 8: Calculated structure of a long cylindrical micelle terminated by a semi-spherical end cap. The dashed line marks the polar-apolar interface, the solid lines indicate the local directions of the surfactant tails. Size mismatch between end cap and cylindrical main body leads to an elastic perturbation that propagates into the cylinder as a damped oscillation with characteristic lengths ξ_1 and ξ_2 given in Eqs. 24.

perturbation that propagates a few nm into the cylindrical main body. The shape shown in Fig. 8 is not based on any structural assumptions other than the requirement that the cylindrical micelle should be end

capped. As in the previous section, the free energy per molecule is modeled as a sum

$$f = \gamma a \left(1 - \frac{a}{a_0}\right)^2 + \tau\gamma a_0 \left(\frac{l - b^\star}{b^\star}\right)^2 \tag{23}$$

of an OFM term for the interfacial forces, and a quadratic term representing the chain stretching energy. In this equation a is the (locally varying) area per headgroup within either the end cap or the perturbed cylindrical part; l is the corresponding *local* average chain length in the two regions, and $b^\star$ denotes the radius corresponding to the minimum of the chain conformational free energy $f_c(b)$ as given in Fig. 3. This value happens to roughly coincide with the optimal tail lengths, b_{sph} and b_{cyl}, in the spherical and cylindrical parts, respectively. (Hence, $b^\star = b_{sph}$ and $b^\star = b_{cyl}$ in their respective regions.) The (dimensionless) chain stretching modulus τ is identical to that introduced in Eq. 20. Note that due to the perturbation of the cylindrical part, the volume-to-surface ratio per amphiphile within the perturbed cylindrical part is not simply $l/2$, but rather depends on the rate at which the average (local) tail length $l(x)$ changes along the micellar axis x, (details can be found in May and Ben-Shaul.[56]) Minimization of the overall free energy shows that the shape of the micellar relaxation profile $l(x)$ is given by a damped oscillation $l(x)/b_{cyl} - 1 \sim \exp(-x/\xi_1)\cos(x/\xi_2)$. The two characteristic length scales are

$$\xi_1 = \frac{b_{cyl}\sqrt{2/3}}{\sqrt{\sqrt{1+\tau} - 1}}, \qquad \xi_2 = \frac{b_{cyl}\sqrt{2/3}}{\sqrt{\sqrt{1+\tau} + 1}} \tag{24}$$

The first, ξ_1, characterizes the exponential decay length of the perturbation; with $b_{cyl} = 16$ Å and $\tau \approx 1$ (both extracted from Fig. 3) we obtain $\xi_1 = 2$ nm. The second, ξ_2, measures the wavelength of oscillations in micellar thickness. For finite τ these oscillations are only noticeable for $x < \xi_1$. In the limiting case that $\tau = 0$, we find that the presence of the spherical end caps induces a periodic oscillation ("pearling") along the micelle axis. This solution for $l(x)$ preserves a constant surface to volume ratio.

At this point we note the close similarity of the present approach with modeling interactions between inclusions in amphiphilic membranes, particularly in lipid membranes. Continuum elasticity theory has frequently been used to calculate the shape profile in the vicinity of one or several symmetric inclusions and the corresponding interaction free energy between inclusions.[60–62] Both the shape profile and the free energy between inclusions as function of their mutual distance are predicted to be described by damped oscillations. This situation is analogous for end capped cylindrical micelles where the end caps play the role of the inclusions and where their elastic interaction is mediated by the cylindrical main body. The damped oscillating free energy found for inclusion-containing membranes is also found for cylindrical micelles, as shown in Fig. 9.

More specifically, Fig. 9 shows the excess free energy μ^0 (calculated according to Eq. 12) of a cylindrical micelle comprising a total of N amphiphiles, relative to the packing free energy that these N amphiphiles would have if they were all packed in the cylindrical body of a very long micelle of optimal thickness b_{cyl}. Hence, μ^0 contains both the energy of forming end caps and their elastic interaction through the cylindrical part of the micelle. In the limit $N \to \infty$ we obtain the energy (2δ) of two individual end caps (corresponding to Fig. 8), including the transition zone between the spherical and cylindrical regions. In the opposite limit, $N = \bar{N} = 60$, the two end caps have merged into a single spherical micelle. Generally, μ^0_{sph} denotes the contribution to the end cap energies stored within the two quasi-spherical cap regions, and $\mu^0_{cyl} = \mu^0 - \mu^0_{sph}$ is the contribution due to the perturbation of the cylindrical part. It is interesting to note that the two contributions are similar in magnitude which underscores the need to include the cylindrical part into the calculation of end cap energies.

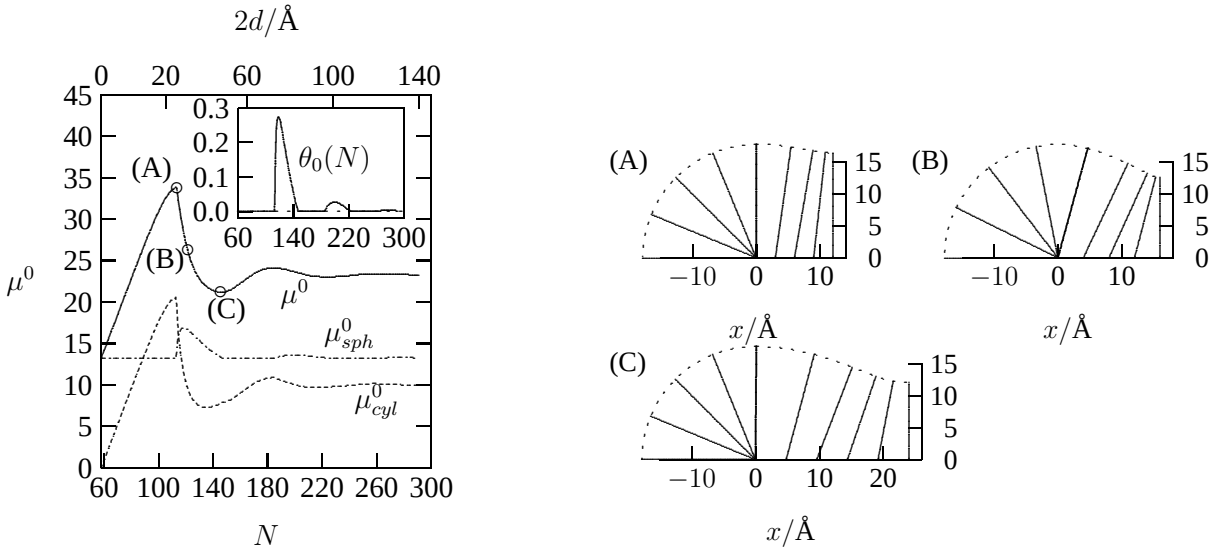

Figure 9: Left diagram: The excess packing free energy (in k_BT's) of amphiphiles in a linear micelle, $\mu^0(N) = \mu^0_{sph}(N_{sph}) + \mu^0_{cyl}(N - N_{sph})$, relative to the energy of packing all N molecules in a cylindrical micelle of optimal thickness b_{cyl}. $\mu^0_{sph}(N_{sph})$ is the contribution due to the N_{sph} molecules constituting the end caps, (relative to N_{sph} molecules in a cylinder of radius b_{cyl}). $\mu^0_{cyl}(N_{cyl})$, with $N_{cyl} = N - N_{sph}$, is defined analogously. Note that N_{sph} varies with N. The calculation is for micelles composed of C-14 amphiphiles, with $\tau = 1$ and preferred packing parameter of $P = \nu/(a_0 b_{max}) = 1/2.5$. The radius of the end cap is $b_{max} = 18$ Å. The inset shows the variation in the contact angle $\theta_0(N)$ (defined in Fig. 7). The three circles on the $\mu^0(N)$ curve specify the aggregation numbers: $N = 113$ (A), $N = 121$ (B), and $N = 146$ (C). The corresponding micellar shapes are shown in the diagrams on the right, where the dashed lines mark the hydrocarbon-water interface. Chain orientations are shown at several arbitrary positions. Adapted from May and Ben-Shaul[56] with permission.

The distance $2d$ between the end caps is roughly proportional to the aggregation number N (for long micelles it is exactly proportional). The right diagram in Fig. 9 shows the micellar shapes corresponding to three selected aggreagtion numbers, $N = 113$, $N = 121$ and $N = 146$. The geometrical shape of a micelle containing $N = 113$ molecules corresponds to a maximum in the aggregate's free energy μ^0. The energetic barrier around this number is about $10\, k_BT$, implying that micelles of aggregation numbers close to this value will be suppressed during micellar growth. This behavior is corroborated by size distributions calculated using Eq. 3, and the function $\mu^0(N)$ in Fig. 9.

In addition to being responsible for the lack of intermediate micellar sizes, the energetic barrier in $\mu^0(N)$ is also responsible for the appearance of a second threshold critical concentration, the second CMC, X_{2c}. To clarify this point it is instructive to divide the micellar size distribution into two populations, short (s) and long (l) micelles, according to

$$X_s = \int_{\bar{N}}^{L} X(N)\, dN, \qquad X_l = \int_{L}^{\infty} X(N)\, dN \tag{25}$$

Here $\bar{N}$ denotes the size of the minimal (spherical) micelle, ($\bar{N} = 60$ in Fig. 9), and L is an aggregation number for which the two end caps do no longer interact with each other (in Fig. 9, $L = 250$ would be a convenient choice). Note that $X(N)$ is determined according to Eq. 3 with $\mu^0(N) = N\tilde{\mu}^0(N)$, as given in

Fig. 9. The two micellar populations are plotted in Fig. 10 as a function of the total amphiphile concentration X. The sharp transition observed for $X = X_{2c}$ is reminiscent of the first CMC as shown in Fig. 1. Here,

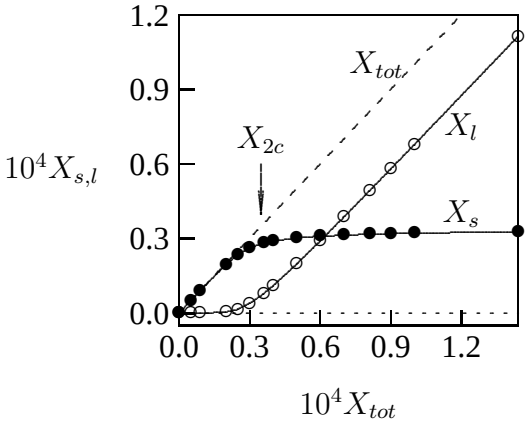

Figure 10: The change in amphiphile populations incorporated in small (X_s) and long (X_l) micelles with the total concentration, X. Small micelles correspond to aggregation numbers $\bar{N} \leq N \leq L = 250$. The dashed line shows $X = X_s + X_l$. The arrow marks the value of the second CMC, X_{2c}, as predicted by Eq. 26. Adapted from May and Ben-Shaul[56] with permission.

however, it separates small, sphere-like micelles from long, cylindrical ones. The weight average of the latter grows, as expected, according to $\langle N \rangle = 2\ \exp(\delta/k_B T)\ \sqrt{X}$ with an end cap energy $\delta = \mu^0_{sph}/2$, (measured relative to the energy of $\bar{N}$ molecules in the optimal cylindrical geometry). The second CMC, X_{2c}, is conveniently defined in analogy to the first, "monomer-to-micelle", CMC, i.e., as the value of X satisfying $(dX_s/dX)_{X_{2c}} = 1/2$. It can be shown that it exists if the excess energy upon approach of the two end caps $g(N) = 2\delta - \mu^0(N)$ has an energetic barrier so that $L^3 \ll \int_{\bar{N}}^{L} dN\ N^2 \exp[g(N)/k_B T]$. In this case the second CMC can be calculated[56] according to

$$X_{2c} = \int_{\bar{N}}^{L} dN\ N e^{-\mu^0(N)/k_B T} \tag{26}$$

The arrow in Fig. 10 marks the position of the second CMC according to this definition. The steep onset of micellar growth at this point is evidenced by the leveling-off in the small micelle population and the linear growth of elongated micelles.

VI. Intermicellar junctions

As briefly discussed in Section II. B., flexible cylindrical micelles can eliminate their end cap energies by forming closed loops, a phenomenon which has been observed experimentally in dilute solutions of micelles involving large end cap energies.[21] At somewhat larger amphiphile concentrations the formation of junctions (that is, branched micelles) provides another way to get rid of energetically unfavorable end caps. Moreover, for an entangled network of worm-like micelles, junctions provide a means to relax stress and thus to reduce viscosity.[63–65]

The formation of a (three-fold) inter-micellar junction may be viewed as a *fusion reaction* between the end cap of one cylindrical micelle with the main body of another, forming a Y-like joint, as illustrated in Fig. 11. Unless they appear already at very low concentrations (thus also leading to network formation) junction formation is energetically unfavorable. Their appearance at higher concentrations may be favored on entropic grounds, due to inter-micellar (primarily excluded volume) interactions , or enhanced by flow fields.[66] Clearly then, the relative magnitudes of the junction formation energy ($\triangle F$) and the end cap excess energy (δ) are crucially important for the structural and dynamic behavior of a micellar solution.

Spherical end caps involve a large positive curvature whereas Y-junctions contain a central part with bilayer-like packing geometry. In Fig. 11 we show the results of molecular-level calculations of the junction formation energy, $\triangle F = F_Y - F_{cyl}$, i.e., the integrated packing energies of the molecules constituting the junction, relative to the energy of the same number of molecules when packed in a cylindrical micelle. Also shown in this figure is the free energy change $\triangle \tilde{F} = \triangle F - \delta$ in the fusion reaction of an end cap with a cylindrical micellar body. In this calculations, as in the two previous sections, the local molecular packing free energy is treated as a sum of a surface energy obeying the OFM and a quadratic chain stretching energy, (see e.g., Eq. 23). As shown in the inset, the junction is treated as composed of three cylinders, joining smoothly into a saddle-like structure. The two structural variables of the junction are the radius r (in the junction plane) of the three semi-toroidal sections connecting the cylinders, and the "pinching factor", α, measuring the thickness of the midpoint, $2b(1-2\alpha)$, relative to the diameter of the cylinder, $2b$. Both r and α are treated as variational parameters. Again we consider C-14 chains, but with varying optimal headgroup areas, as dictated by the interaction parameter B introduced in Section III.

From Fig. 4 we know that a rather wide range of headgroup repulsion parameters $B_{min} < B < B_{max}$ favor the formation of cylindrical aggregates. Values close to the transition to spherical micelles ($B \lesssim B_{max}$) imply small end cap energy and large Y-junction energy. On the other hand, proximity to the transition into a lamellar structure ($B_{min} \lesssim B$) suggests that the fusion reaction displayed in Fig. 11 could be energetically favorable. Consistent with that notion, several (mixed) bilayer systems that underwent a transition towards

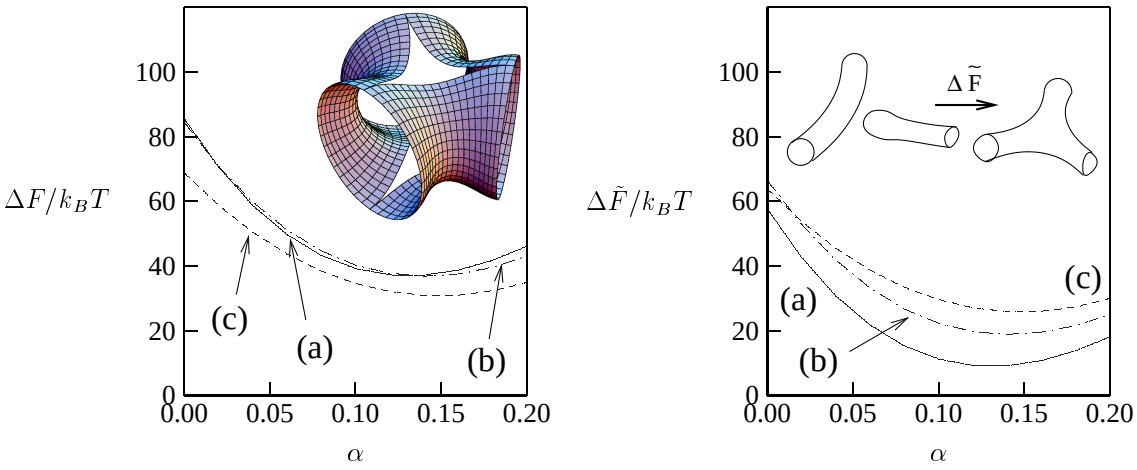

Figure 11: Left diagram: The energy $\triangle F$ of forming a Y-junction from an unperturbed cylinder of optimal thickness b. The three different curves correspond to different headgroup repulsion parameters: $B = 270 k_B T \text{Å}^2$ (a), $B = 330 k_B T \text{Å}^2$ (b), and $B = 450 k_B T \text{Å}^2$ (c). They are shown as function of the pinching factor α which specifies the decrease in thickness of the junction's middle part. The inset shows the structural model for the optimal Y-junction, corresponding to $B = 270 k_B T \text{Å}^2$ and $\alpha = 0.13$. Right diagram: The energy $\triangle \tilde{F}$ of forming a Y-junction via a fusion reaction between a cylindrical micelle and an end cap. The three curves correspond to the same B values as in the left diagram. The fusion reaction is schematically depicted in the right diagram. Adapted from May *et al*[30] with permission.

a micellar phase were recently found to disintegrate into a network-like structure of branched cylindrical micelles with large junction density and no apparent end caps.[67,68] Y-junctions have also been observed using Cryo-TEM for several other surfactants, including alkylamine oxide and alkyl ethoxylate sulfate mixtures at high pH or salt conditions,[69] the nonionic surfactant $C_{12}E_5$,[51] and a trimeric surfactant.[70] Moreover, imaging evidence exists for the formation of branched micelles and network-like structures for diblock

copolymer blends.[55,71] Here, the individual micelles were found unable to exchange monomers but could relax into a state of local equilibrium subject to their quenched topological structure. Due to their larger size (as compared to surfactant micelles) Cryo-TEM images of the copolymer micelles revealed a remarkable number of subtle structural details, including enlarged end caps that induce damped elastic undulations of the cylindrical main body, even more pronounced than those displayed in Fig. 8. Moreover, short micellar branches exhibited a quantized length distribution, corresponding to discrete multiples of the undulation wave length. This observation is consistent with our previous remark that when $\tau = 0$ micelles of integer multiples of ξ_2 (see Eq. 24) are characterized by the same area-to-volume ratio.

Micellar phases that form randomly connected networks are able to exhibit a (first order) transition into two coexisting phases of different surfactant concentration. Such a transition was already noted by Appell and Porte[72] for cetylpyridinium chlorate in high salt conditions and suggested to arise from network formation due to micellar branching.[19,73] Early theoretical and computer simulation studies supported this hypothesis.[74] Branching was also observed in Cryo-TEM studies[51] for the nonionic micelles of $C_{12}E_5$ (and for mixtures of $C_{12}E_5$ with a nonionic phospholipid[75]). These studies reveal coexistence between a concentrated and a a dilute network of interconnected cylindrical micelles. The generality of this transition for self-assembling networks that allow the formation of n-fold junctions ($n = 1, 2, 3, \dots$) was recently recognized by Tlusty and Safran.[76] Indeed, similar transitions (involving the coexistence of two networks of different density, of one network with a phase of disjointed chains, or of two disjointed chain phases with different degree of branching[77]) are also found for microemulsions[51] and might be present in dipolar fluids.[78,79] The phase transition was suggested to be purely entropic;[74,77] its driving force is the large entropy of the junction-dominated phase. A complementary view, namely the condensation of chains driven by a favorable energy of junction formation, was recently advanced and supported through Monte-Carlo simulations by Kindt.[80]

The packing of the amphiphiles in a Y-junction is, on average, intermediate between that in a bilayer and a cylindrical micelle. This is because the junction may be, approximately, regarded as consisting of a small central bilayer-like region surrounded by three semi-toroidal sections. The latter can be viewed as three highly bent semi-cylindrical micelles, implying a cylinder-like packing geometry in these regions (the bending introduces saddle curvatures which further reduce the average curvature in these parts). Consistent with this notion, junctions predominantly appear for systems where amphiphile packing energies in cylinders and planar bilayers are not too different. In analogy to the micellar end cap (see Fig. 8), there is a mismatch between the preferred thicknesses of the bilayer-like and the bent semi-cylindrical regions. As indicated in the right diagram of Fig. 4, amphiphiles subject to cylindrical packing conditions tend to adopt a larger aggregate thickness $2b$ compared to the bilayer-like packing geometry. Hence, one expects the central bilayer part in a Y-junction to be pinched downward. Returning to Fig 11 we note that the optimal geometry of the Y-junction is indeed obtained for a positive pinching factor α, implying thinning of the middle part of the junction relative to the diameters of the joining cylinders.[30] The structures of the Y-junctions obtained by these variational calculations reveal a weak dependence of the junction energy on the headgroup repulsion parameter B. Furthermore, in all cases the minimum was adopted for a pinching parameter $\alpha \approx 0.13$; see Fig. 11. Notably, in all these calculations the fusion reaction appears to involve a small, yet positive, energetic penalty for the formation of a Y-junction; e.g., $\triangle\tilde{F} \approx 10\, k_BT$ for $B = 270\, k_BT\text{Å}^2$. Note, however, that even though junction formation may be energetically unfavorable, excluded volume interactions and network entropy considerations may drive their appearance at high concentrations or as transient, metastable, structures. It will be interesting to test other models (such as the continuum model[56] used to derive the end cap structure in Fig. 8) with respect to predicting negative $\triangle\tilde{F}$.

VII. Electrostatic properties of cylindrical micelles

Numerous surfactants carry ionic headgroups, such as sulphate and ammonium salts, carboxylic acids and a multitude of others ionizable groups. Electrostatic repulsion between their charged headgroups tend to increase the optimal area per molecule, a_0, at the hydrocarbon-water interface of an amphiphilic aggregate. Consequently, single-tail ionic surfactants are typically characterized by a small packing parameter $P = \nu/(a_0 b_{max}) < 1/3$, explaining their pronounced preference to form small globular micelles. Nevertheless, many ionic surfactants are also involved in the formation of cylindrical, even worm-like, micelles. The growth of spherical into cylindrical micelles, indicating a packing parameter in the range $1/3 < P < 1/2$, may be due to a number of reasons, e.g., a large tail volume ν, as in the case of gemini surfactants, or the use of strongly binding counterions.[10,81] Effective "charge dilution" by mixing anionic and cationic surfactants,[82] or ionic and zwitterionic (e.g., bile salt and lecithin) amphiphiles can also lead to the appearance of worm-like micelles. And, of course, growth of ionic micelles can also be enhanced by the classical method for screening electrostatic interactions, namely, by adding salt.

To account for the influence of electrostatic interactions on micellar growth we should include their contribution, f_{el}, in the overall free energy per amphiphile in a micelle, f. For simplicity, let us assume, as in the simple OFM, that f_c is constant, and suppose further that non-electrostatic repulsions between headgroups (e.g., those due to excluded volume and hydration forces) are adequately described by the term B/a, so that $f = \gamma a + B/a + f_{el}$; see Eq. 13. Based on the linearized Poisson-Boltzmann theory, the electrostatic (charging) free energy per headgroup is given by $f_{el} = 2\pi k_B T l_B l_D/a$, and thus depends on the Bjerrum length, l_B, and the Debye screening length, l_D. (This result is valid for charges on a planar interface, such as that of a lipid bilayer. We ignore here the weak dependence of f_{el} on surface curvature.) The Bjerrum length, $l_B = e^2/(4\pi\epsilon_0\epsilon_W k_B T)$, measures the distance over which the interaction between two elementary charges e equals the thermal energy $k_B T$ (note that ϵ_0 is the permittivity of free space). In an aqueous solution of dielectric constant $\epsilon_W = 80$ its value is $l_B \approx 7$Å. The Debye length $l_D = (8\pi l_B n_0)^{-1/2}$ is the distance beyond which electrostatic interactions (here in a symmetric 1:1 electrolyte present with bulk concentration n_0) are effectively screened. Using $f = \gamma a + B/a + 2\pi k_B T l_B l_D/a$, we now find

$$a_0 = [(B + 2\pi l_B l_D k_B T)/\gamma]^{(1/2)}. \tag{27}$$

As expected, the preferred area per headgroup is enhanced by electrostatic interactions, and depends strongly on the salt concentration in solution. For example, reducing n_0 from 1 M to 1 mM (corresponding to an increase of the Debye length from $l_D = 3$ Å to $l_D = 100$ Å) implies a corresponding change of the preferred headgroup area from $a_0 = 50$ Å^2 to $a_0 = 200$ Å^2. This crude estimate is certainly oversimplified, yet it clearly demonstrates the major role played by electrostatic interactions in determining the behavior of ionic surfactant solutions.

The long-range nature of the Coulomb potential plays a direct role in determining various structural characteristics (e.g., the persistence length) of worm-like micelles, as well as rheological and thermodynamic properties which are influenced by inter-micellar interactions. Many of these properties have been studied in detail, both experimentally and theoretically. A number of authors have included electrostatic and non-electrostatic interactions in self-consistent theoretical treatments of micelle formation and growth.[83–85] Below, we briefly outline some qualitative theoretical aspects concerning the influence of ionic interactions on the growth of cylindrical micelles.

The spatial distribution of counterions around the surface of a self-assembled macroion depends on its geometry. The counterions released from ionizable groups spread on planar surfaces, such as ionic lipid bilayers, are always largely immobilized, remaining close to the surface, thus forming a diffuse layer of

finite thickness. On the other hand, spherical macroions never immobilize their counterions. Cylindrical macroions exhibit an intermediate behavior: depending on their line charge density, a certain fraction of the counterions may remain close to their surface. Quite generally then, *counterion condensation*[86,87] on charged surfaces is a geometry-dependent phenomenon.[88] Of greatest relevance to the behavior of ionic worm-like micelles is, of course, the distribution of counterions around charged cylindrical macroions.

For a (long) cylinder there is a critical line charge density λ (the number of charges per unit length along the cylinder) above which counterion condensation sets in. Specifically, if $\xi = \lambda l_B$ (known as the Manning parameter) exceeds unity ($\xi > 1$), a fraction of counterions $1 - 1/\xi$ stays in close proximity (that is closer than a distance R_M away from the rod) and cannot be diluted away. The effective average line charge density along the cylinder axis is thus $\hat{\lambda} = e/l_B$. The concept of counterion condensation remains valid for salt-containing solutions as long as R_M is smaller then the Debye length.[89] The implications of counterion condensation have been extensively studied for DNA, in which case $\xi = 4.2$ implies that a large fraction of the counterions are in fact condensed on the DNA rod. Cylindrical micelles are often more strongly charged and should thus exhibit substantial condensation. Consider for example a cylindrical micelle of radius $b = 16$ Å composed of amphiphiles whose area per head group is $a = 50$ Å^2. If all these headgroups were ionized, the line charge density along the micelle axis would be $\lambda = 2\pi be/a$, implying $\xi = 2\pi b l_B/a = 14$, which is considerably larger than that of DNA.

The notion of counterion condensation appears also in the work of Safran *et al*[90] and MacKintosh *et al*,[91] who studied the influence of electrostatic interactions on the growth characteristics of worm-like micelles. In their model there are two populations of counterions. Those that condense on the micelle surface thus reducing the "bare" line charge density along the micellar axis to $\hat{\lambda} = e/l_B$. The rest of the counterions are free and uniformly spread in solution and thus provide a constant contribution to the electrostatic free energy of the system, independent of the micellar size distribution. On the other hand, the size distribution is strongly affected by the Coulomb forces between the ("effective") bare charges along the micelle backbone. The electrostatic interaction energy between two neighboring charges is small, just $1\, k_BT$, but owing to the very long range of the Coulomb interaction, the electrostatic free energy of a micelle is much larger due to significant contributions from distant charges charges along the micelle axis.

The length of a cylindrical micelle of radius b containing N molecules of area a is $L = (a/2\pi b)N$, and the number of effective bare charges is $L/l_B = \hat{\lambda}L/e$. Integrating over all pairwise Coulomb potentials in this micelle it can be shown that $\mu^0_{el}(N)$, the electrostatic contribution to the packing free energy of the micelle, is given by

$$\mu^0_{el}(N) = k_BTc\,[N\ln(cN) - N] \tag{28}$$

where $c = a/(2\pi b l_B)$ is a dimensionless constant. (The factor k_BT replaces here $e^2/4\pi\epsilon_0\epsilon_W l_B$ the electrostatic interaction energy between two neighboring charges). The positive nonlinear electrostatic term $\sim N\ln N$ acts against $N\mu^0_{cyl}$, the (negative) linear contribution to $\mu^0(N)$ which arises from molecular packing in the cylindrical body and encourages micellar growth; as discussed in detail in Section II.B.. Adding the electrostatic contribution above we now have $\mu^0(N) = N\mu^0_{cyl} + k_BTc\,[N\ln(cN) - N] + \delta$. Using this expression in the micellar growth formalism of Section II, it can be shown that the two competing tendencies imply that in dilute solutions of ionic micelles most micelles are of roughly the same length $L^\star$, in marked contrast to the polydisperse size distribution of neutral micelles. More explicitly, the size distribution is sharply peaked around a specific $N^\star = (2\pi b/a)L^\star$, which grows only weakly with X, according to the solution of the equation $N^\star = [2\delta + \ln(X/N^\star)]/ck_BT$.

This behavior prevails at low concentrations, as long as the micelles do not yet "overlap" in space. A measure for the overlap concentration is provided by the 'mesh-size' of a solution of (long, randomly oriented) rodlike particles, which is $\tilde{L} \sim b/\sqrt{\phi}$ for rods of radius b, where $\phi = X(\nu/\nu_w)$ is the volume

fraction of micelles in solution. Once $L^\star$ reaches $\tilde{L}$ the system enters the semi-dilute regime. Now, any given micelle charge sees, on average, an electrically neutral environment at distances $L > \tilde{L} = b/\sqrt{\phi}$, so that electrostatic interactions (along the micelle axis) beyond this distance are effectively screened. The functional form of Eq. 28 for $\mu^0_{el}(N)$ is still valid, except that N should be replaced by $\tilde{N} = (2\pi b/a)\tilde{L} = (2\pi b^2/a)/\sqrt{\phi}$. Thus, now $\mu^0_{el}(N) = k_BT(l_Bb/a)\sqrt{\phi}\left[\ln(l_Bb/a)\sqrt{\phi}) - 1\right]$ is independent of N and affects the size distribution only through the total amphiphile concentration $X = (\nu_w/\nu)\phi$. The electrostatic contribution now simply rescales the growth parameter δ to a lower value,

$$\delta_{eff} = \delta - k_BT\frac{l_Bb\lambda^2}{\sqrt{X}} \tag{29}$$

resulting in lower average micellar size, $\langle N\rangle = 2\sqrt{X}\exp(\delta_{eff}/k_BT)$, as compared to that of neutral micelles.

MacKintosh *et al*[91] have also analyzed the influence of added salt on the micellar growth characteristics. They predict that addition of salt (with intermediate or large concentration $n_0 \gg 1/(8\pi l_B L^2)$) is equivalent to increasing the total amphiphile mole fraction by $8\pi l_B b^2 n_0$, thus enhancing micellar growth. Qualitatively, this effect represents more efficient screening of the charges at the cylindrical body, as compared to the spherical end caps. Additional experiments are needed in order to test the various theoretical predictions outlined above. So far direct experimental information is rather limited. Under salt free conditions it was found, for instance, that cationic gemini surfactants exhibit a multi-modal population of aggregates.[9]

Another property that is affected by electrostatic interactions is the persistence length $\xi = \xi_0 + \xi_{el}$ of a worm-like micelle. The theoretical basis for assessing their influence has been provided by Odijk[92] and Skolnick and Fixman[93] (OSF). Based on the linearized, Debye Hückel, limit of Poisson-Boltzmann theory, these authors derived an explicit expression $\xi_{el} = l_Bl_D^2/(4l^2)$ for the electrostatic contribution to ξ of an intrinsically rigid polymer (ξ_0 is the non-electrostatic contribution to the persistence length). Non-linear Poisson-Boltzmann theory was used by Le Bret[94] and Fixman[95] who considered charged cylinders with low inner dielectric constant and initially uniform surface charge density. The result for ξ_{el} turned out to depend on the relaxation parameter η (see also Eq.19) which describes how the charge density changes upon bending. Reasonable agreement with OSF was found for $\eta = b/3$. Generally, experimental determinations of the persistence length of charged worm-like micelles are also in agreement with the OSF predictions.[36,46,47] Yet, on the more theoretical level, there is no consensus regarding the correct scaling of ξ_{el} with the Debye length l_D for flexible polyelectrolytes, as recently discussed by Dobrynin and Rubinstein.[12] At this point, computer simulations provide powerful tools to test the relation $\xi_{el}(l_D)$,[48,96] as well as to account for intermicellar interactions and the polydisperse character of solutions of reversibly assembling worm-like micelles.[46] What may also be important at this point is the indirect influence of electrostatic interactions on ξ_0. This influence is expressed in a number of counterion-specific effects that have been observed experimentally.[10,81] To illustrate a possible mechanism recall that Eq. 22 predicts the non-electrostatic contribution to the persistence length ξ of a worm-like micelle to scale with the aggregate thickness $2b$ like $\xi_0 \sim b^3$. Changes due to electrostatic interactions of the cross-sectional area per amphiphile in a cylindrical micelle $a_0 \sim b^{-1}$ will thus be reflected in ξ_0.

ACKNOWLEDGMENTS

SM thanks the support from ND ERSCoR through NSF grant #EPS-01232289. ABS thanks the support of the Israel Science Foundation (ISF grant #227/02), the US-Israel Binational Science Foundation (BSF grant #2002-75), and the Archie and Marjorie Sherman Chair. The Fritz Haber Center is supported by the Minerva Foundation, Munich, Germany.

References and Notes

1. Evans, D. F.; Wennerström, H. *The colloidal domain, where physics, chemistry, and biology meet;* VCH publishers: , Second ed.; 1994.
2. Gelbart, W. M.; Ben-Shaul, A. *J. Chem. Phys.* **1996,** *100,* 13169-13189.
3. Safran, S. A. *Statistical thermodynamics of surfaces, interfaces, and membranes;* Addison-Wesley: New York, 1994.
4. Gelbart, W. M.; Ben-Shaul, A.; Roux, D., Eds.; *Micelles, Membranes, Microemulsions and Monolayers,* ; Springer: Berlin, 1994.
5. Cates, M. E.; Candau, S. J. *J. Phys. Cond. Matter.* **1990,** *2,* 6869-6882.
6. Bombelli, F. B.; Berti, D.; Pini, F.; Keiderling, U.; Baglioni, P. *J. Phys. Chem. B* **2004,** *108,* 16427–16434.
7. LaRue, I.; Adam, M.; Silva, M. D.; Sheiko, S. S.; Rubinstein, M. *Macromolecules* **2004,** *37,* 5002–5005.
8. Oda, R.; Lequeux, F.; Mendes, E. *J. Phys. II France* **1996,** *6,* 1429-1439.
9. Weber, V.; Narayanan, T.; Mendes, E.; Schosseler, F. *Langmuir* **2003,** *19,* 992–1000.
10. Magid, L. J. *J. Phys. Chem. B* **1998,** *102,* 4064–4074.
11. Dobrynin, A. V. *Macromolecules* **2005,** *38,* 9304–9314.
12. Dobrynin, A. V.; Rubinstein, M. *Prog. Polym. Sci.* **2005,** *30,* 1049-1118.
13. Israelachvili, J. N. *Intermolecular and Surface Forces;* Academic Press: , Second ed.; 1992.
14. Israelachvili, J. N.; Mitchell, J.; Ninham, B. W. *J. Chem. Soc. Farad. 2* **1976,** *72,* 1525–1568.
15. Ben-Shaul, A. Molecular theory of chain packing, elasticity and lipid protein interaction in lipid bilayers. In *Structure and Dynamics of Membranes*, Vol. 1; Lipowsky, R.; Sackmann, E., Eds.; Elsevier: Amsterdam, 1995.
16. Paula, S.; Süs, W.; Tuchtenhagen, J.; Blume, A. *J. Phys. Chem.* **1995,** *99,* 11742-11751.
17. Tanford, C. *The Hydrophobic Effect;* Wiley-Interscience: New-York, 2 ed.; 1980.
18. Israelachvili, J. N.; Mitchell, J.; Ninham, B. W. *Biophys. Biochim. Acta.* **1977,** *470,* 185–201.
19. Porte, G. Micellar Growth, Flexibility and Polymorphism in Dilute Solutions.. In *Micelles, Membranes, Microemulsions, and Monolayers*, First ed.; Gelbart, W. M.; Ben-Shaul, A.; Roux, D., Eds.; Springer: New York, 1994.
20. Van Der Schoot, P.; Wittmer, J. P. *Macrom. Theory Sim.* **1999,** *8,* 428–432.
21. In, M.; Aguerre-Chariol, O.; Zana, R. *J. Phys. Chem. B* **1999,** *103,* 7747–7750.

22. Bernheim-Groswasser, A.; Zana, R.; Talmon, Y. *J. Phys. Chem.B* **2000,** *104,* 4005–4009.

23. Zhu, J.; Liao, Y.; Jiang, W. *Langmuir* **2004,** *20,* 3809–3812.

24. Harries, D.; Ben-Shaul, A. *J. Chem. Phys.* **1997,** *106,* 1609–1619.

25. Benshaul, A.; Szleifer, I. *J.Chem.Phys.* **1985,** *83,* 3597-3611.

26. Ben-Shaul, A.; Gelbart, W. M. Statistical thermodynamics of amphiphile self-assembly: Structure and phase transitions in micellar solutions. In *Micelles, Membranes, Microemulsions, and Monolayers*, First ed.; Gelbart, W. M.; Ben-Shaul, A.; Roux, D., Eds.; Springer: New York, 1994.

27. Fattal, D. R.; Ben-Shaul, A. *Biophys. J.* **1993,** *65,* 1795–1809.

28. May, S.; Ben-Shaul, A. *Phys. Chem. Chem. Phys.* **2000,** *2,* 4494–4502.

29. Flory, P. J. *Statistical mechanics of chain molecules;* Wiley-Interscience: New-York, 1969.

30. May, S.; Bohbot, Y.; Ben-Shaul, A. *J. Phys. Chem. B* **1997,** *101,* 8648–8657.

31. Grosberg, A.; Khokhlov, A. *Statistical Physics of Macromolecules;* AIP PRess: New York, 1994.

32. Rubinstein, M.; Colby, R. *Polymer physics;* Oxford University Press: New York, 2003.

33. Boal, D. *Mechanics of the Cell;* Cambridge University Press: , 2001.

34. Lipowsky, R.; Sackmann, E., Eds.; *Structure and Dynamics of Membranes,* ; Elsevier: Elsevier, Amsterdam, 1995.

35. Helfrich, W. *Z. Naturforsch.* **1973,** *28,* 693–703.

36. Magid, L. J.; Li, Z.; Butler, P. D. *Langmuir* **2000,** *16,* 10028–10036.

37. May, S. Unpublished data.

38. Fournier, J. B. *Europhys. Lett.* **1998,** *43,* 725–730.

39. Hamm, M.; Kozlov, M. M. *Eur. Phys. J. E* **2000,** *3,* 323–335.

40. Hamm, M.; Kozlov, M. M. *Eur. Phys. J. B* **1998,** *6,* 519–528.

41. May, S. *Eur. Biophys. J.* **2000,** *29,* 17–28.

42. Lauw, Y.; Leermakers, F. A. M.; Stuart, M. A. C. *J. Phys. Chem. B* **2003,** *107,* 10912–10918.

43. Imae, T. *Colloid Polym. Sci.* **1989,** *267,* 707–713.

44. Von Berlepsch, H.; Harnau, L.; Reineker, P. *J. Phys. Chem. B* **1998,** *102,* 7518–7522.

45. Geng, Y.; Ahmed, F.; Bhasin, N.; Discher, D. E. *J. Phys. Chem. B* **2005,** *109,* 3772–3779.

46. Jerke, G.; Pedersen, J. S.; Egelhaaf, S. U.; Schurtenberger, P. *Langmuir* **1998,** *14,* 6013–6024.

47. Schubert, B. A.; Kaler, E. W.; Wagner, N. J. *Langmuir* **2003,** *19,* 4079–4089.

48. Cannavacciuolo, L.; Pedersen, J. S.; Schurtenberger, P. *Langmuir* **2002,** *18,* 2922–2932.

49. Porte, G.; Poggi, Y.; Appell, J.; Maret, G. *J. Phys. Chem.* **1984,** *88,* 5713–5720.

50. Geng, Y.; Romsted, L. S.; Menger, F. *J. Am. Chem. Soc.* **2006,** *128,* 492–501.

51. Bernheim-Groswasser, A.; Wachtel, E.; Talmon, Y. *Langmuir* **2000,** *16,* 4131–4140.

52. Glatter, O.; Fritz, G.; Lindner, H.; Brunner-Popela, J.; Mittelbach, R.; Strey, R.; Egelhaaf, S. U. *Langmuir* **2000,** *16,* 8692–8701.

53. Gonzlez-Prez, A.; Varela, L. M.; García, M.; Rodríguez, J. R. *J. Coll. Int. Sci.* **2006,** *293,* 213–221.

54. Zheng, Y.; Won, Y.; Bates, F. S.; Davis, H. T.; Scriven, L. E.; Talmon, Y. *J. Phys. Chem. B* **1999,** *103,* 10331–10334.

55. Jain, S.; Bates, F. S. *Macromolecules* **2004,** *37,* 1511–1523.

56. May, S.; Ben-Shaul, A. *J. Phys. Chem. B* **2001,** *105,* 630–640.

57. Bauer, A.; Woelki, S.; Kohler, H. H. *J. Phys. Chem. B* **2004,** *108,* 2028–2037.

58. Kshevetskiy, M. S.; Shchekin, A. K. *Coll. J.* **2005,** *67,* 324–336.

59. Al-Anber, Z. A.; Josep Bonet i Avalos, J.; Floriano, M. A.; Mackie, A. D. *J. Chem. Phys.* **2003,** *118,* 3816–3826.

60. Dan, N.; Pincus, P.; Safran, S. A. *Langmuir* **1993,** *9,* 2768–2771.

61. Nielsen, C.; Goulian, M.; Andersen, O. S. *Biophys. J.* **1998,** *74,* 1966–1983.

62. May, S.; Ben-Shaul, A. *Biophys. J.* **1999,** *76,* 751–767.

63. Appell, J.; Porte, G.; Kathory, A.; Kern, F.; Candau, S. J. *J. Phys. II France* **1992,** *2,* 1045–1052.

64. Khatory, A.; Kern, F.; Lequeux, F.; Appell, J.; Porte, G.; Morie, N.; Ott, A.; Urbach, W. *Langmuir* **1993,** *9,* 933–939.

65. Buhler, E.; Munch, J. P.; Candau, S. J. *Europhys. Lett.* **1996,** *34,* 251–255.

66. Bruinsma, R.; Gelbart, W. M.; Ben-Shaul, A. *J. Chem. Phys.* **1992,** *96,* 7710-7727.

67. Gustafsson, J.; Oradd, G.; Lindblom, G.; Olsson, U.; Almgren, M. *Langmuir* **1997,** *13,* 852–860.

68. Gustafsson, J.; Oradd, G.; Nyden, M.; Hansson, P.; Almgren, M. *Langmuir* **1998,** *14,* 4987–4996.

69. Lin, Z. *Langmuir* **1996,** *12,* 1729-1737.

70. Danino, D.; Talmon, Y.; Levy, H.; Beinert, G.; Zana, R. *Science* **1995,** *269,* 1420–1421.

71. Jain, S.; Bates, F. S. *Science* **2003,** *300,* 460–464.

72. Appell, J.; Porte, G. *J. Phys. (France)* **1983,** *44,* 689–695.

73. Gomati, R.; Appell, J.; Bassereau, P.; Marignan, J.; Porte, G. *J. Phys. Chem.* **1987,** *91,* 6203–6210.

74. Bohbot, Y.; Ben-Shaul, A.; Granek, R.; Gelbart, W. M. *J. Chem. Phys.* **1995,** *103,* 8764-8782.

75. Kwon, S. Y.; Kim, M. W. *Phys. Rev. Lett.* **2002,** *89,* 258302/1–258302/4.

76. Tlusty, T.; Safran, S. A. *Science* **2000,** *290,* 1328-1331.

77. Zilman, A.; Tlusty, T.; Safran, S. A. *J. Phys. Cond. Mat.* **2003,** *15,* S57–S64.

78. Camp, P. J.; Shelley, J. C.; Patey, G. N. *Phys. Rev. Lett.* **2000,** *84,* 115–118.

79. Weis, J. J.; Tavares, J. M.; Gama, M. M. T. D. *J. Phys. Cond. Mat.* **2002,** *14,* 9171–9186.

80. Kindt, J. T. *J. Phys. Chem. B* **2002,** *106,* 8223–8232.

81. Magid, L. J.; Han, Z.; Li, Z.; Butler, P. D. *J. Phys. Chem. B* **2000,** *104,* 6717–6727.

82. Koehler, R. D.; Raghavan, S. R.; Kaler, E. W. *J. Phys. Chem. B* **2000,** *104,* 11035–11044.

83. Evans, D. F.; Mitchel, D. J.; Ninham, B. W. *J. Phys. Chem.* **1984,** *88,* 6344–6349.

84. Nagarajan, R.; Ruckenstein, E. *Langmuir* **1991,** *7,* 2934–2969.

85. Srinivasan, V.; Blankschtein, D. *Langmuir* **2003,** *19,* 9932–9945.

86. Oosawa, F. *Polyelectrolytes;* Marcel Mecker, New-York: , Second ed.; 1970.

87. Manning, G. S. *Q. Rev. Biophys.* **1978,** *11,* 179–246.

88. Belloni, L. *Colloid Surf. A* **1998,** *140,* 227–243.

89. Deserno, M.; Holm, C.; May, S. *Macromolecules* **2000,** *33,* 199–205.

90. Safran, S. A.; Pincus, P. A.; Cates, M. E.; MacKintosh, F. C. *J. Phys. France* **1990,** *51,* 503–510.

91. MacKintosh, F. C.; Safran, S. A.; Pincus, P. A. *Europhys. Lett.* **1990,** *12,* 697–702.

92. Odijk, T. *J. Polym. Sci. Part B: Polym. Phys.* **1977,** *15,* 477-483.

93. Skolnick, J.; Fixman, M. *Macromolecules* **1977,** *10,* 944-948.

94. Le Bret, M. *J. Phys. Chem.* **1982,** *76,* 6243.

95. Fixman, M. *J. Phys. Chem.* **1982,** *76,* 6346–6353.

96. Everaers, R.; Milchev, A.; Yamakov, V. *Eur. Phys. J.* **2002,** *8,* 3-13.